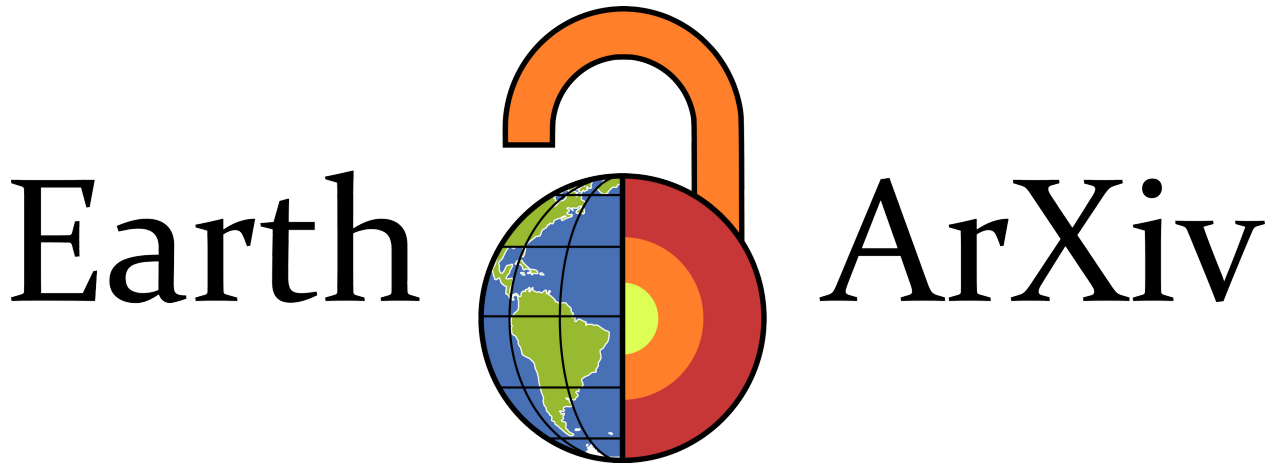

Recent intensification of eastern Pacific ENSO is unprecedented across the last millennium

Authors: J.E. Cole[1]*, D.M. Thompson[2], K.A. Dyez[1], C.J. Tripp[1], A.W. Tudhope[3], M. Lofverstrom[2], S. Stevenson[4], J.M. Okun[1], A.E. Lawman[5], J.L. Conroy[6], J.T. Overpeck[7], G. Jimenez[8], R.L. Edwards[9]

Affiliations:

[1]Department of Earth and Environmental Sciences, University of Michigan; Ann Arbor, MI, 48109, USA

[2] Department of Geosciences, University of Arizona; Tucson, AZ, 85721, USA

[3] School of GeoSciences, University of Edinburgh; EH9 3FE, Scotland, UK

[4] Bren School of Environmental Sciences & Management, University of California; Santa Barbara, CA, 93106, USA

[5] Environmental Studies and Science Program, Colorado College; Colorado Springs, CO, 80903, US

[6] Department of Earth Science & Environmental Change, University of Illinois at Urbana-Champaign; Urbana, IL, 61801, USA

[7] School of Environment and Sustainability, University of Michigan; Ann Arbor, MI, 48109, USA

[8]

[9] Department of Earth and Environmental Sciences, University of Minnesota; Minneapolis, MN, 55455, USA

* Corresponding author. Email: colejul@umich.edu.

Abstract: The Pacific El Niño-Southern Oscillation (ENSO) phenomenon generates climate extremes that endanger ecosystems, infrastructure, and human well-being worldwide. The response of this system to climate warming is poorly constrained, due to data scarcity and climate model biases, making projections of future climate hazards uncertain. The geochemistry of Galápagos coral skeletons across the past millennium reveals an unprecedented increase in interannual variability of sea surface temperature in the eastern equatorial Pacific that has emerged above pre-industrial levels and exceeds simulated natural variability. This increase parallels the rise in global temperature and results from stronger El Niño events. Central Pacific coral data also show increased variability, although less distinctly than in Galápagos. Our results provide long-term context for understanding ENSO variability trends, with troubling implications for future climate extremes.

Main text:

El Niño-Southern Oscillation (ENSO) is the leading source of interannual extremes in modern climate, linked to droughts, floods, infrastructural damages, coral bleaching, wildfires, and agricultural and health impacts (*1-3*). ENSO is defined by coupled variability of the ocean and atmosphere in the equatorial Pacific, emerging from multiple physical processes as a coherent pattern of interannual changes in tropical Pacific sea surface temperature (SST) and associated wind, hydrologic, and oceanographic features (*4, 5*). The complexity of the system, and influences from other regions (*6*), create large internal variability that masks a clear response to external climate forcing (*7, 8*). The lack of long-term observations from the core ENSO region, together with ambiguities in climate model projections, motivates this development of paleoclimate records from Galápagos corals (Fig. 1, S1) to quantify recent changes in ENSO variability in the context of the past millennium.

Spatial and temporal ENSO variability

Recent decades have experienced several large and impactful El Niño events, with warming that extends from the South American coast to the dateline. Warm anomalies centered in the eastern Pacific (EP events) are typically stronger than those focused in the central Pacific (CP events) (*9, 10*) and those concentrated along the tropical South American coastline (coastal El Niño) (*11*). These spatial modes of ENSO may respond differently to changing climate forcing, as assessed over recent millennia (*12, 13*), and under anthropogenic influences (*5, 14, 15*). The large internal variability of ENSO, together with the sparse instrumental record of the remote equatorial Pacific (*16*) (fig. S2), makes it difficult to attribute the recent recurrence of strong El Niño events unequivocally to anthropogenic warming (*17, 18*). The increase in strong, basin-wide El Niño events in recent decades is reflected in the rising trend of skewness in eastern Pacific SST anomaly data (*15, 19*) (fig. S2).

Model projections of future climate change have historically not agreed on whether ENSO SST variability would weaken or strengthen in a warming climate. Using the latest generation of coupled climate models (phases 5 and 6 of the Coupled Model Intercomparison Project, hereafter CMIP5 and CMIP6), the Intergovernmental Panel on Climate Change found no consensus on changing variability in a standard index of central Pacific (Niño3.4) SST, even under high emissions scenarios (*7*). Complicating factors include inter-model differences in reproducing key ENSO metrics; internal variability that masks forced responses; non-monotonic responses of variability across the 21st century; and spatial biases that undermine comparisons with geographically fixed indices (*20-23*).

Model studies that attempt to control for some of these issues tend to simulate increased ENSO SST variability under anthropogenic forcing. Large ensembles of forced simulations using CMIP6 models mostly show increasing ENSO SST variance through the 21st century (*20, 24*). However, the spatial and temporal expressions of this change differ among models, implying diverse mechanisms. In CMIP5-6 models that distinguish EP and CP modes, the increase in ENSO variance is strongest, and emerges sooner, in the EP relative to the CP (*15, 25*). Despite

the developing view that ENSO SST variability is likely to increase under anthropogenic forcing, the underlying mechanisms and time-evolving trajectories of variance differ among models, highlighting that we still lack an unambiguous physical understanding of the simulated changes (*26*).

The spatial and temporal limitations of the instrumental SST record restrict our ability to assess long-term changes in ENSO. The first systematic SST observations of the remote regions that define ENSO variability (e.g. Niño 3.4: 5°S-5°N; 120-180°W) only began in the 1980s with satellite observations, later augmented by the in-situ TOGA-TAO array (*1*). Gridded instrumental SST products differ in their representations of tropical Pacific SST variability during periods of low observations (fig. S2). Thus, high-resolution paleoclimate data from the tropical Pacific play a particularly useful role in defining long-term baselines and patterns of ENSO variability (*27-31*).

ENSO paleo-records from Galápagos corals

Here we use a collection of modern and subfossil Galápagos coral samples to quantify changes in interannual SST variance across the past millennium in the eastern equatorial Pacific (table S1). The Galápagos archipelago lies in the heart of the EP mode of ENSO variability (fig. S3), where the strongest basin-wide ENSO extremes create maximum SST anomalies and have the greatest impacts globally. Interannual variability in Galápagos SST (figs. 1, S1) is directly tied to ENSO dynamics through changes in thermocline depth and upwelling, and secondarily through advection. Coral skeletal Sr/Ca and $\delta^{18}O$ are well-established tracers of past SST in Galápagos (*32-35*). In the central archipelago, seawater $\delta^{18}O$ ($\delta^{18}O_{sw}$) reflects circulation changes rather than freshwater balance (*36*), does not correlate with ENSO indices or local SST (Thompson and Conroy et al. 2022). We demonstrate that $\delta^{18}O_{coral}$ shows high reproducibility among records and strong agreement with local SST patterns, supporting their interpretation as ENSO-sensitive temperature records.

We use coral Sr/Ca and $\delta^{18}O$ to characterize SST variations over the past millennium (Methods). These proxies correlate well ($p < 0.001$) with local SST and indices of EP-ENSO variability (fig. S3, S4). Our results derive from the analysis of 28 time series sampled at 5 islands across the Galápagos archipelago (fig. S1, tables S1-S3; figs. S5-S6), using local SST-geochemistry calibrations (table S4). We apply an empirical correction to account for gradients of SST mean and variability across our sampling area (figs. S1, S7; table S3). These precisely dated, sub-seasonal records complement lower resolution records from eastern tropical Pacific sedimentary archives (*37-39*), coral-based ENSO reconstructions from other Pacific regions (*28-30*), multiproxy and multicoral syntheses (*8, 14, 40-42*), and measures of teleconnected ENSO impact (*43, 44*).

We calculate a metric of interannual SST variability based on filtered bimonthly SST anomalies reconstructed from coral Sr/Ca and $\delta^{18}O$ (Methods). Using this measure, we quantify

the change in variability from a modern benchmark period (tables 1, S5) and compare our results to coral data from the central Pacific (CP; fig. 1, table S6), the Indo-Pacific warm pool, and against multi-proxy and multi-site ENSO reconstructions. We use forced and unforced simulations of the Community Earth System Model (v1.2) Last Millennium Ensemble (CESM-LME) (*45*) as a benchmark against which to assess coral results over the last millennium and explore simulated anthropogenic trends (see Methods).

Results: Increasing variability in eastern Pacific SST

Over the past millennium, the history of EP-ENSO variability at Galápagos parallels global temperature and reveals a striking amplification in the last ~40 years (figs. 2, 3). Relatively low and consistent variance characterizes the first 850 years of the record (1000-1850 CE, hereafter "pre-industrial"). In the period that follows (1850-1981; hereafter "20th century"), variability begins to rise in the late 19th century, emerging clearly above the preindustrial range by the late 20th century. The range of SST variability in the "modern" interval (here defined as after 1984) is almost entirely above that reconstructed during the preindustrial period. Across the instrumental period, reconstructed variability closely tracks the rising trend in variability and skewness (fig. 2, S8) of EP SST that stems from more frequent strong El Niño events. Over the past millennium, the coral data show increasingly positive skewness that accompanies the rise in variability, pointing to stronger warm events as the driver for increased variance (fig. S9). Unusual SST variance in the eastern equatorial Pacific thus has emerged from the background state of this naturally dynamic system.

Each of the three intervals that we define (fig. 2; pre-industrial, 20th-century, and modern) exhibits variance that is statistically distinct from the others, increasing through time (T-test; $p \leq 0.01$). Using the percent change in standard deviation, normalized to a recent benchmark 20-yr interval (Methods), we find that modern EP ENSO is 37 (±8)% stronger than that of the pre-industrial, and that 20th-century EP ENSO is 16 (±9)% stronger than preindustrial (table 1). Values in parentheses reflect the standard deviation among estimates from individual cores. Modern and 20th-century samples derive exclusively from the two most northern islands in the Galápagos (Wolf and Darwin), and preindustrial samples derive mostly from the main archipelago (fig. S1). Geographic normalization (Methods) corrects for underlying variability differences among the sites that are largely due to upwelling (fig. S7), but even without this correction the modern epoch exhibits significantly higher variability ($p<0.05$) than the earlier intervals (fig. S10). Data from Isla Wolf include the preindustrial, 20th-century, and modern epochs, confirming the dramatic increase in SST variability at one site.

Our new analysis of last-millennium $\delta^{18}O$ data from Line Islands corals extends and largely agrees with earlier work (*29*) that documents a recent increase in CP ENSO variability. Before 1850 CE, the range of variability is larger in the Line Islands than in the Galápagos, and the preindustrial variability overlaps with modern ranges in some cases (fig. 3). Nevertheless, the mean increase in Line Islands variability from pre-industrial to modern epochs, 38 (±12)%, is

consistent with that seen in Galápagos, and the mean values in each epoch are statistically distinct (table 1).

Fossil coral studies from Sumatra and Vanuatu (*30, 46*) show increasing interannual variance over the past millennium that has been interpreted as ENSO-related. The changes in variability reconstructed from individual cores fall in the same range as the data from Galápagos and the northern Line Islands, but do not show the clear distinction between preindustrial and modern samples that emerges from the Galápagos data (fig. S11). Analysis of continuous ENSO reconstructions that use coral, tree-ring and other paleodata (*14, 42, 43*) show a rise in variance in the mid-19th century (fig S12) that precedes the Galápagos pattern, and variability across the past millennium exhibits a wider range than in the EP.

Analysis of simulated EP ENSO variability using all members of the fully forced, preindustrial CESM-LME simulations (*45*) reveals that the pre-industrial to modern change in Galápagos SST variability stands out as significant ($p < 0.05$) against the simulated background of naturally forced variability (fig. 4). The variability change reconstructed from Galápagos corals lies above the 95% significance level compared to both the fully forced ensemble (36%) and the unforced control run (30%; fig. S13; table S7). Using the 4 LME ensemble members that extend to CE 2100 with anthropogenic forcings, we find a 95% confidence limit of 33%, also below the level of change reconstructed at Galápagos.

Spatial diversity in the evolution of ENSO variance

Over the past millennium, the eastern and central Pacific reconstructions agree on the amplitude of ENSO variance change, and neither indicates significant variability changes associated with the Little Ice Age (ca. 1500-1850 CE) or Medieval (ca. 800-1350 CE) (*47*) eras. However, these reconstructions differ in other ways. The Galápagos coral analysis reveals a tight range of preindustrial variability across cores and sites, and a strong distinction between modern/20th century and preindustrial variability. By contrast, the central Pacific coral records show larger differences among cores in the variability of ENSO throughout the preindustrial, and therefore a less distinct emergence of recent changes in ENSO statistics.

Several explanations may account for this difference between eastern and central Pacific coral reconstructions. Conceivably, gaps in datasets could create such differences; the Galápagos data sample 51% of the years in the 1047-2014 interval, and the Line Islands sample 59% of this interval. Alternatively, Pacific decadal variability may impact the Line Islands more so than Galápagos, as its imprint is stronger in the CP (*10, 48, 49*). Although we filter decadal and longer variability from each individual record, this would not erase inter-core contrasts that could result from multidecadal variability.

More likely, this difference may reflect the mix of factors that determine coral $\delta^{18}O$ records in the EP and CP. In the Line Islands, $\delta^{18}O_{sw}$ varies with both freshwater balance and circulation, and typically amplifies the coral $\delta^{18}O$ signal that results from ENSO SST variability. Interannual SST anomalies are relatively small, and the coral $\delta^{18}O$ signal includes a substantial seawater $\delta^{18}O$ component (*50, 51*)). By contrast, in Galápagos, interannual SST changes are sufficiently large that they dominate the coral $\delta^{18}O$ signal, as supported by good agreement between paired $\delta^{18}O$ and Sr/Ca records and long-term $\delta^{18}O_{sw}$ monitoring. Seawater $\delta^{18}O$ reflects circulation-driven salinity changes that do not correlate with local SST or ENSO indices (*36*).

To the extent that these coral records reflect variability in EP (Galápagos) and CP (Line Islands) ENSO SST, they suggest a response to external forcing that is consistent with model inferences. In several comprehensive analyses, CMIP5-6 models tend to project forced increases in ENSO SST variability that is more consistent and emerges more rapidly in the EP than in the CP (Cai et al., 2018; Geng et al., 2022). This pattern can result from several interrelated features, among them a reduced zonal SST gradient, increased stratification due to warming and intensified rainfall, and the nonlinear Bjerknes feedback associated with eastern Pacific warming (*20, 23-25*). The coral reconstructions do not distinguish among mechanisms, but do provide an independent set of observations that confirm widely simulated patterns.

Comparison with continuous ENSO reconstructions

The continuous ENSO reconstructions (*14, 42, 43*) suggest that ENSO variability began to increase before 1900, prior to substantial warming (fig. S12). This timing contrasts with the mid-20th century increase seen at Galápagos, and may reflect biases that would be expected to create this particular timing. First, small age model errors of as little as a year can cause misalignment of extreme years among records, reducing interannual variance as age model errors accumulate downcore (*40, 52*). The start of instrumental SST records in the mid-19th century provides a point of comparison for coral data that can reduce such errors starting at that time. Second, records from the equatorial Pacific (±5° latitude), where core ENSO variance dominates, virtually all begin between 1850-1900 CE; reconstructed interannual variance therefore increases as these records are added to the reconstructions (*40*). The age model bias is minimized in the case of tree-ring-only ENSO reconstructions (*43*), but the scarcity of old tropical tree-ring records remains a source of inhomogeneity. A third bias results from using extratropical and terrestrial records that may be nonlinearly or inconsistently related to equatorial Pacific SST (*53-55*). Prior to the late 19th century, these reconstructions do not agree consistently in the timing of changes in variability.

Fossil coral reconstructions lack the continuity of multi-site paleoclimate syntheses, but they provide an alternate and compelling view of last-millennium ENSO variability that sidesteps these inherent biases. The Galápagos data – although sparse in the 19th century – indicate that the largest increase in EP-ENSO SST variability did not begin until the mid-late 20th century, coincident with accelerated global warming (fig. 3).

Comparison with simulated ENSO variability

The reconstructed increase in EP-ENSO SST variability is highly unusual ($p < 0.05$), compared to the variability simulated by the fully forced CESM-LME for the pre-industrial period (850-1850 CE) (fig. 4). To assess the role of natural forcing, we compare the Galápagos results to the variance distributions from millennium-long fully-forced and unforced (control) simulations from the same model (fig. S13). The variability is only slightly larger in the forced simulation ensemble than in the control for the intervals sampled by the corals, and is the same when the full simulation lengths are considered (table S7). These results support previous suggestions that natural radiative forcings over the past millennium have not contributed substantially to ENSO variability (*12, 28*).

In the 4 LME ensemble members that extend to 2100 CE with anthropogenic forcing (RCP8.5), higher variance tends to occur in the 21st century, although it appears later than in our coral records and is not consistently above earlier levels (fig. S14). In the CESM-LME, internal variability appears to play a larger role than external forcing. In contrast with the Galápagos coral results, simulated EP SST variability in the 21st century does not emerge above the background of pre-industrial conditions. The CESM-LME may thus overestimate internal variability, while underestimating the response to anthropogenic forcing, in the EP region.

Conclusions

We document an unambiguous increase in EP ENSO SST variance since 1850, particularly in recent decades, that cannot be ascribed to internal variability or natural forcings and that reflects the observed intensification of El Niño warm extremes. This amplification is consistent with Earth system model projections that ENSO-related SST variance is likely to increase and will be detectable first in the eastern Pacific (*20, 25*). However, our data show that increased SST variance in the EP is emerging from background variability more rapidly than expected from model simulations, whereas in the CP, increasing variance has not clearly emerged above that of the past millennium. The use of seasonally resolved paleoclimate data allows us to describe a natural pre-industrial range of EP-ENSO SST variability across a time span vastly longer than the instrumental record, highlighting the unprecedented nature of recent EP SST variability compared to the past millennium. We find scant evidence for coherent century-scale changes in Galápagos SST variability prior to the industrial era, suggesting that the Little Ice Age and Medieval climate eras have no relationship to the strength of EP ENSO variability.

These results have important implications for future climate hazards. ENSO extremes regularly impose tremendous economic costs, ecological damages, and human suffering (*2, 3*). The impact of more frequent and extreme El Niño events, superimposed on background ocean warming, has been particularly devastating to coral reef ecosystems in recent decades, and will

continue to wreak changes upon marine ecosystems more broadly (*56-58*). Greater ENSO variance will affect global teleconnections: as climate warms, the hydroclimatic impacts of ENSO are expected to amplify regardless of changes in SST variability (*59*). Our results highlight that the underlying SST variability is also strengthening, which will further intensify the impact of ENSO within and beyond the tropical Pacific. By demonstrating a clear increase in eastern Pacific ENSO variability under recent unprecedented anthropogenic forcing, our results provide a point of comparison for identifying climate model simulations that successfully capture this change, which may improve our ability to anticipate and prepare for future risks.

References and Notes

1. M. J. McPhaden, T. Lee, S. Fournier, M. A. Balmaseda, in *El Niño Southern Oscillation in a Changing Climate,* M. McPhaden, A. Santoso, W. Cai, Eds. (American Geophysical Union, Washington DC, 2020), pp. 39-63.
2. L. Goddard, A. Gershunov, in *El Niño Southern Oscillation in a Changing Climate,* M. McPhaden, A. Santoso, W. Cai, Eds. (American Geophysical Union, Washington DC, 2020), pp. 361-375.
3. P. Lehodey *et al.*, in *El Niño Southern Oscillation in a Changing Climate,* M. McPhaden, A. Santoso, W. Cai, Eds. (American Geophysical Union, Washington DC, 2020), pp. 429-451.
4. M. Collins *et al.*, The impact of global warming on the tropical Pacific ocean and El Nino. *Nature Geoscience* **3**, 391-397 (2010).
5. W. J. Cai *et al.*, Changing El Nino-Southern Oscillation in a warming climate. *Nature Reviews Earth & Environment* **2**, 628-644 (2021).
6. W. J. Cai *et al.*, Pantropical climate interactions. *Science* **363**, 944-+ (2019).
7. J. Y. Lee *et al.*, in *Climate Change 2021: The Physical Science Basis. Contribution of Working Group I to the Sixth Assessment Report of the Intergovernmental Panel on Climate Change,* P. Z. V. Masson-Delmotte, A. Pirani, S. L. Connors, C. Péan, S. Berger, N. Caud, Y. Chen, L. Goldfarb, M. I. Gomis, M. Huang, K. Leitzell, E. Lonnoy, J. B. R. Matthews, T. K. Maycock, T. Waterfield, O. Yelekçi, R. Yu, and B. Zhou, Ed. (Cambridge University Press, Cambridge, United Kingdom and New York, NY, USA, 2021).
8. J. Emile-Geay, K. M. Cobb, J. E. Cole, M. Elliot, F. Zhu, in *El Niño Southern Oscillation in a Changing Climate,* M. McPhaden, A. Santoso, W. Cai, Eds. (American Geophysical Union, Washington DC, 2020), pp. 87-118.
9. J. S. Kug, F. F. Jin, S. I. An, Two Types of El Nino Events: Cold Tongue El Nino and Warm Pool El Nino. *Journal of Climate* **22**, 1499-1515 (2009).
10. A. Capotondi, A. T. Wittenberg, J.-S. Kug, K. Takahashi, M. J. McPhaden, in *El Niño Southern Oscillation in a Changing Climate,* M. McPhaden, A. Santoso, W. Cai, Eds. (American Geophysical Union, Washington DC, 2020), pp. 65-86.
11. K. Takahashi, A. G. Martínez, The very strong coastal El Nino in 1925 in the far-eastern Pacific. *Climate Dynamics* **52**, 7389-7415 (2019).
12. S. Stevenson, A. Capotondi, J. Fasullo, B. Otto-Bliesner, Forced changes to twentieth century ENSO diversity in a last Millennium context. *Climate Dynamics* **52**, 7359-7374 (2017).

13. C. Karamperidou, P. N. DiNezio, Holocene hydroclimatic variability in the tropical Pacific explained by changing ENSO diversity. *Nat Commun* **13**, 7244 (2022).
14. M. B. Freund *et al.*, Higher frequency of Central Pacific El Nino events in recent decades relative to past centuries. *Nature Geoscience* **12**, 450-+ (2019).
15. W. J. Cai *et al.*, Increased variability of eastern Pacific El Nino under greenhouse warming. *Nature* **564**, 201-+ (2018).
16. C. Deser, A. S. Phillips, M. A. Alexander, Twentieth century tropical sea surface temperature trends revisited. *Geophysical Research Letters* **37**, (2010).
17. B. Wang *et al.*, Historical change of El Nino properties sheds light on future changes of extreme El Nino. *Proc Natl Acad Sci U S A* **116**, 22512-22517 (2019).
18. R. Gan, Q. Liu, G. Huang, K. Hu, X. Li, Greenhouse warming and internal variability increase extreme and central Pacific El Niño frequency since 1980. *Nature Communications* **14**, 394 (2023).
19. H. Y. Kao, J. Y. Yu, Contrasting Eastern-Pacific and Central-Pacific Types of ENSO. *Journal of Climate* **22**, 615-632 (2009).
20. W. J. Cai *et al.*, Anthropogenic impacts on twentieth-century ENSO variability changes. *Nature Reviews Earth & Environment* **4**, 407-418 (2023).
21. S. Stevenson, A. T. Wittenberg, J. Fasullo, S. Coats, B. Otto-Bliesner, Understanding Diverse Model Projections of Future Extreme El Nino. *Journal of Climate* **34**, 449-464 (2021).
22. U. K. Heede, A. V. Fedorov, N. J. Burls, Time Scales and Mechanisms for the Tropical Pacific Response to Global Warming: A Tug of War between the Ocean Thermostat and Weaker Walker. *Journal of Climate* **33**, 6101-6118 (2020).
23. H. B. Fredriksen, J. Berner, A. C. Subramanian, A. Capotondi, How Does El Nino-Southern Oscillation Change Under Global Warming-A First Look at CMIP6. *Geophysical Research Letters* **47**, (2020).
24. N. Maher *et al.*, The future of the El Nino-Southern Oscillation: using large ensembles to illuminate time-varying responses and inter-model differences. *Earth System Dynamics* **14**, 413-431 (2023).
25. T. Geng *et al.*, Emergence of changing Central-Pacific and Eastern-Pacific El Nino-Southern Oscillation in a warming climate. *Nat Commun* **13**, 6616 (2022).
26. U. K. Heede, A. V. Fedorov, Towards understanding the robust strengthening of ENSO and more frequent extreme El Nino events in CMIP6 global warming simulations. *Climate Dynamics* **61**, 3047-3060 (2023).
27. F. E. Urban, J. E. Cole, J. T. Overpeck, Modification of tropical Pacific variability by its mean state inferred from a 155 year coral record. *Nature* **407**, (2000).
28. K. M. Cobb *et al.*, Highly Variable El Nino-Southern Oscillation Throughout the Holocene. *Science* **339**, 67-70 (2013).
29. P. R. Grothe *et al.*, Enhanced El Nino-Southern Oscillation Variability in Recent Decades. *Geophysical Research Letters* **47**, (2019).
30. A. E. Lawman *et al.*, A Century of Reduced ENSO Variability During the Medieval Climate Anomaly. *Paleoceanography and Paleoclimatology* **35**, (2020).
31. I. S. Nurhati, K. M. Cobb, E. Di Lorenzo, Decadal-Scale SST and Salinity Variations in the Central Tropical Pacific: Signatures of Natural and Anthropogenic Climate Change. *Journal of Climate* **24**, 3294-3308 (2011).

32. R. B. Dunbar, G. M. Wellington, M. W. Colgan, P. W. Glynn, Eastern Pacific sea surface temperature since 1600 A.D.: The d18O record of climate variability in Galapagos corals. *Paleoceanography* **9**, 291-316 (1994).
33. J. E. Cole, A. W. Tudhope, in *Coral Reefs of the Eastern Tropical Pacific: Persistence and Loss in a Dynamic Environment,* P. W. Glynn, D. P. Manzello, I. C. Enochs, Eds. (Springer Science+Business Media, Dordrecht, 2017), vol. 8, pp. 535-548.
34. G. Jimenez, J. E. Cole, D. M. Thompson, A. W. Tudhope, Northern Galapagos Corals Reveal Twentieth Century Warming in the Eastern Tropical Pacific. *Geophysical Research Letters* **45**, 1981-1988 (2018).
35. A. H. Cheung *et al.*, Fidelity of the Coral Sr/Ca Paleothermometer Following Heat Stress in the Northern Galapagos. *Paleoceanography and Paleoclimatology* **36**, (2021).
36. J. L. Conroy *et al.*, Equatorial Undercurrent Influence on Surface Seawater δ18O Values in the Galápagos. *Geophysical Research Letters* **50**, e2022GL102074 (2023).
37. G. T. Rustic, A. Koutavas, T. M. Marchitto, B. K. Linsley, Dynamical excitation of the tropical Pacific Ocean and ENSO variability by Little Ice Age cooling. *Science* **350**, 1537-1541 (2015).
38. D. M. Thompson *et al.*, Tropical Pacific climate variability over the last 6000 years as recorded in Bainbridge Crater Lake, Galapagos. *Paleoceanography* **32**, 903-922 (2017).
39. J. L. Conroy, J. T. Overpeck, J. E. Cole, T. M. Shanahan, M. Steinitz-Kannan, Holocene changes in eastern tropical Pacific climate inferred from a Galapagos lake sediment record. *Quaternary Science Reviews* **27**, 1166-1180 (2008).
40. G. Loope, D. Thompson, J. Cole, J. Overpeck, Is there a low-frequency bias in multiproxy reconstructions of tropical pacific SST variability? *Quaternary Science Reviews* **246**, (2020).
41. S. McGregor, A. Timmermann, M. H. England, O. E. Timm, A. T. Wittenberg, Inferred changes in El Nino-Southern Oscillation variance over the past six centuries. *Climate of the Past* **9**, 2269-2284 (2013).
42. J. Emile-Geay, K. M. Cobb, M. E. Mann, A. T. Wittenberg, Estimating Central Equatorial Pacific SST Variability over the Past Millennium. Part II: Reconstructions and Implications. *Journal of Climate* **26**, 2329-2352 (2013).
43. J. B. Li *et al.*, El Nino modulations over the past seven centuries. *Nature Climate Change* **3**, 822-826 (2013).
44. Y. Liu *et al.*, Recent enhancement of central Pacific El Nino variability relative to last eight centuries. *Nature Communications* **8**, (2017).
45. B. L. Otto-Bliesner *et al.*, Climate variability and change since 850 CE An ensemble approach with the Community Earth System Model. *Bulletin of the American Meteorological Society* **97**, 735-754 (2016).
46. N. J. Abram *et al.*, Coupling of Indo-Pacific climate variability over the last millennium. *Nature* **579**, 385-+ (2020).
47. M. E. Mann *et al.*, Global Signatures and Dynamical Origins of the Little Ice Age and Medieval Climate Anomaly. *Science* **326**, 1256-1260 (2009).
48. M. Newman *et al.*, The Pacific Decadal Oscillation, Revisited. *Journal of Climate* **29**, 4399-4427 (2016).
49. A. Sullivan *et al.*, Robust contribution of decadal anomalies to the frequency of central-Pacific El Nino. *Scientific Reports* **6**, (2016).

50. D. M. Thompson *et al.*, Identifying hydro-sensitive coral δ18O records for improved high-resolution temperature and salinity reconstructions. *Geophysical Research Letters*, e2021GL096153 (2022).
51. S. Stevenson *et al.*, Contrasting Central Equatorial Pacific Oxygen Isotopic Signatures of the 2014/2015 and 2015/2016 El Niño Events. *Geophysical Research Letters* **50**, e2023GL104454 (2023).
52. M. Comboul *et al.*, A probabilistic model of chronological errors in layer-counted climate proxies: applications to annually banded coral archives. *Climate of the Past* **10**, 825-841 (2014).
53. J. E. Cole, E. R. Cook, The changing relationship between ENSO variability and moisture balance in the continental United States. *Geophysical Research Letters* **25**, 4529-4532 (1998).
54. A. J. E. Gallant, S. J. Phipps, D. Karoly, A. B. Mullan, A. M. Lorrey, Non-stationary Australasian teleconnections and implications for paleoclimate reconstructions. *Journal of Climate* **26**, 8827-8849 (2013).
55. S. C. Lewis, A. N. LeGrande, Stability of ENSO and its tropical Pacific teleconnections over the Last Millennium. *Clim. Past* **11**, 1347-1360 (2015).
56. T. M. Clarke *et al.*, Linking observed changes in pelagic catches to temperature and oxygen in the Eastern Tropical Pacific. *Fish and Fisheries* **23**, 1371-1382 (2022).
57. N. J. Holbrook *et al.*, Keeping pace with marine heatwaves. *Nature Reviews Earth & Environment* **1**, 482-493 (2020).
58. T. P. Hughes *et al.*, Spatial and temporal patterns of mass bleaching of corals in the Anthropocene. *Science* **359**, 80-+ (2018).
59. S. Power, F. Delage, C. Chung, G. Kociuba, K. Keay, Robust twenty-first-century projections of El Nino and related precipitation variability. *Nature* **502**, 541-+ (2013).
60. R. W. Reynolds *et al.*, Daily high-resolution-blended analyses for sea surface temperature. *Journal of Climate* **20**, 5473-5496 (2007).
61. N. A. Rayner *et al.*, Global analyses of sea surface temperature, sea ice, and night marine air temperature since the late nineteenth century. *Journal of Geophysical Research: Atmospheres* **108**, (2003).
62. R. Neukom *et al.*, Consistent multidecadal variability in global temperature reconstructions and simulations over the Common Era. *Nature Geoscience* **12**, 643-+ (2019).
63. K. Cowtan, R. G. Way, Coverage bias in the HadCRUT4 temperature series and its impact on recent temperature trends. *Quarterly Journal of the Royal Meteorological Society* **140**, 1935-1944 (2014).
64. E. R. M. Druffel, S. Griffin, D. Vetter, R. B. Dunbar, D. M. Mucciarone, Identification of frequent La Niña events during the early 1800s in the east equatorial Pacific. *Geophysical Research Letters* **42**, 1512-1519 (2015).
65. E. V. Reed *et al.*, Impacts of Coral Growth on Geochemistry: Lessons From the Galapagos Islands. *Paleoceanography and Paleoclimatology* **36**, (2021).
66. H. Cheng *et al.*, Improvements in Th-230 dating, Th-230 and U-234 half-life values, and U-Th isotopic measurements by multi-collector inductively coupled plasma mass spectrometry. *Earth and Planetary Science Letters* **371**, 82-91 (2013).
67. P. W. Glynn, State of Coral Reefs in the Galapagos Islands: Natural vs Anthropogenic Impacts. *Mar. Pollut. Bull.* **29**, 131-140 (1994).

68. P. W. Glynn, B. Riegl, A. M. S. Correa, I. B. Baums, Rapid recovery of a coral reef at Darwin Island, Galapagos Islands. *Galapagos Research* **66**, 6-13 (2009).
69. K. Thirumalai, A. Singh, R. Ramesh, A MATLAB™ code to perform weighted linear regression with (correlated or uncorrelated) errors in bivariate data. *Journal of the Geological Society of India* **77**, 377-380 (2011).
70. G. M. Wellington, R. B. Dunbar, G. Merlen, Calibration of stable oxygen isotope signatures in Galápagos corals. *Paleoceanography* **11**, 467-480 (1996).
71. A. Capotondi, ENSO diversity in the NCAR CCSM4 climate model. *J. Geophys. Res.-Oceans* **118**, 4755-4770 (2013).
72. B. Huang *et al.*, NOAA Extended Reconstructed Sea Surface Temperature (ERSST), Version 5: Upgrades, validations, and intercomparisons. *Journal of Climate*, (2017).
73. A. H. Jaffey, K. F. Flynn, L. E. Glendenin, W. C. Bentley, A. M. Essling, PRECISION MEASUREMENT OF HALF-LIVES AND SPECIFIC ACTIVITIES OF U-235 AND U-238. *Physical Review C* **4**, 1889-+ (1971).
74. S. C. Sanchez *et al.*, A Continuous Record of Central Tropical Pacific Climate Since the Midnineteenth Century Reconstructed From Fanning and Palmyra Island Corals: A Case Study in Coral Data Reanalysis. *Paleoceanography and Paleoclimatology* **35**, (2020).
75. K. M. Cobb, C. D. Charles, H. Cheng, R. L. Edwards, El Nino/Southern Oscillation and tropical Pacific climate during the last millennium. *Nature* **424**, 271-276 (2003).
76. I. S. Nurhati, K. M. Cobb, C. D. Charles, R. B. Dunbar, Late 20th century warming and freshening in the central tropical Pacific. *Geophysical Research Letters* **36**, (2009).
77. S. G. Dee *et al.*, No consistent ENSO response to volcanic forcing over the last millennium. *Science* **367**, 1477-+ (2020).
78. K. M. Cobb, C. D. Charles, D. E. Hunter, A central tropical Pacific coral demonstrates Pacific, Indian, and Atlantic decadal climate connections. *Geophysical Research Letters* **28**, 2209-2212 (2001).
79. L. K. Zaunbrecher *et al.*, Coral records of central tropical Pacific radiocarbon variability during the last millennium. *Paleoceanography* **25**, (2010).
80. M. Evans, R. G. Fairbanks, J. L. Rubenstone, A proxy index of ENSO teleconnections. *Nature* **394**, 732-733 (1998).

Acknowledgments: We are deeply grateful to the Galápagos National Park, particularly G. Quezada, D. Rueda, and J. Suarez, for permission to work in this special place, and to the Charles Darwin Research Station, notably M. Romoleroux, S. Cisneros, and S. Rea, for facilitating this work. We could not have done this project without robust field support from L. Cruz, R. Pepolas, and E. Romero. We appreciate field and lab support from S. Hlohowskyj, M. Wilson, D. Ruiz, S. Lemieux, M. Nicholson, S. Acosta, D. Dettman, C. Garton, C. Kotila, J. McCraw, and M. Snyder.

Funding: Provide complete funding information, including grant numbers, complete funding agency names, and recipient's initials. Each funding source should be listed in a separate paragraph.

US National Science Foundation grants OCE 0957881, OCE 1401326, OCE 1829613 (JEC).

US National Science Foundation grant AGS 1561121 (DMT)

US National Science Foundation grant AGS 2002460 (DMT and ML)

US National Science Foundation grant AGS 1847791 (JLC)

US National Science Foundation grants OCE 2142953, OCE 2202794, AGS 1805143 (SS)

UK Natural Environmental Research Council grant NERC NE/H009957/1 (AWT)

Author contributions:

Conceptualization: JEC, AWT, DMT

Funding acquisition: JEC, AWT, DMT

Methodology: JEC, DMT, AWT, SS

Formal Analysis: JEC, CJT, DMT, ML, AEL, JMO

Investigation: KAD, JMO, GJ, RLE, JEC

Visualization: JEC, KAD, DMT

Project administration: JEC

Supervision: JEC

Writing – original draft: JEC, DMT, SS, ML. KAD

Writing – review & editing: all authors

Competing interests: Authors declare that they have no competing interests.

Data and materials availability: All data will be made available through the NOAA-National Centers for Environmental Information Paleoclimatology web site (link to be provided on publication).

Supplementary Materials

Materials and Methods
Figs. S1 to S14
Tables S1 to S7
References 60-80

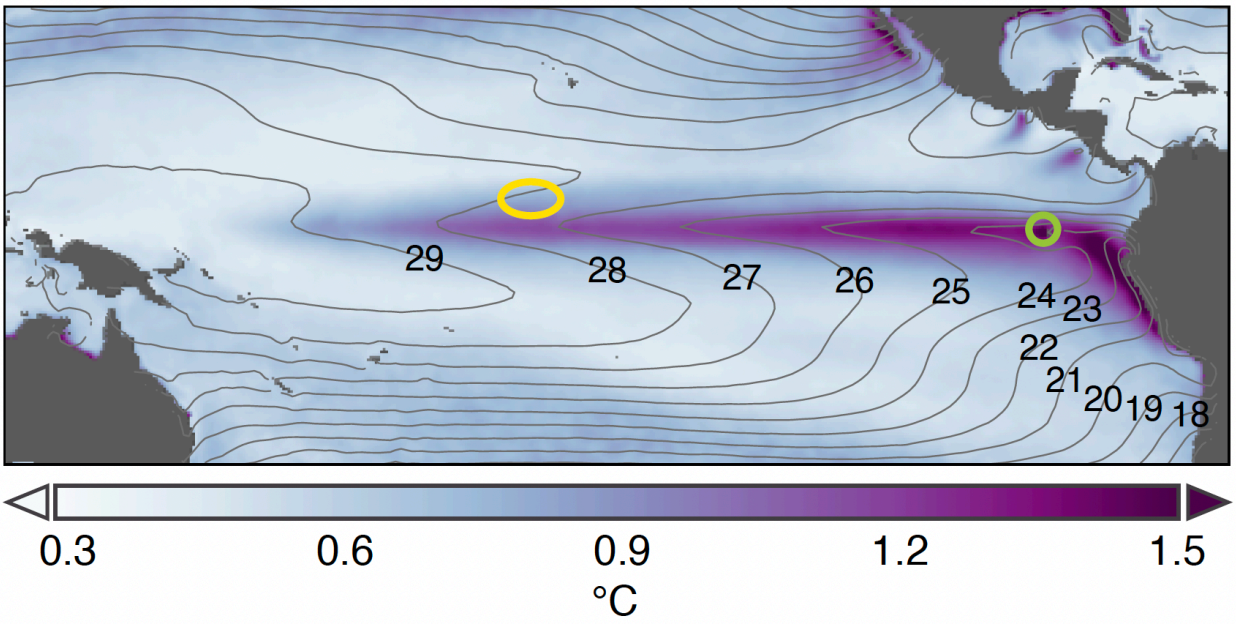

Figure 1. Standard deviation of observed monthly SST anomalies (1982-2024; colors), superimposed on mean SST (labeled contours in °C). The Galápagos and Line Island archipelagos are indicated by green and yellow symbols, respectively. Data accessed from OISSTv2.1 product (*60*) using Climate Explorer (https://climexp.knmi.nl/).

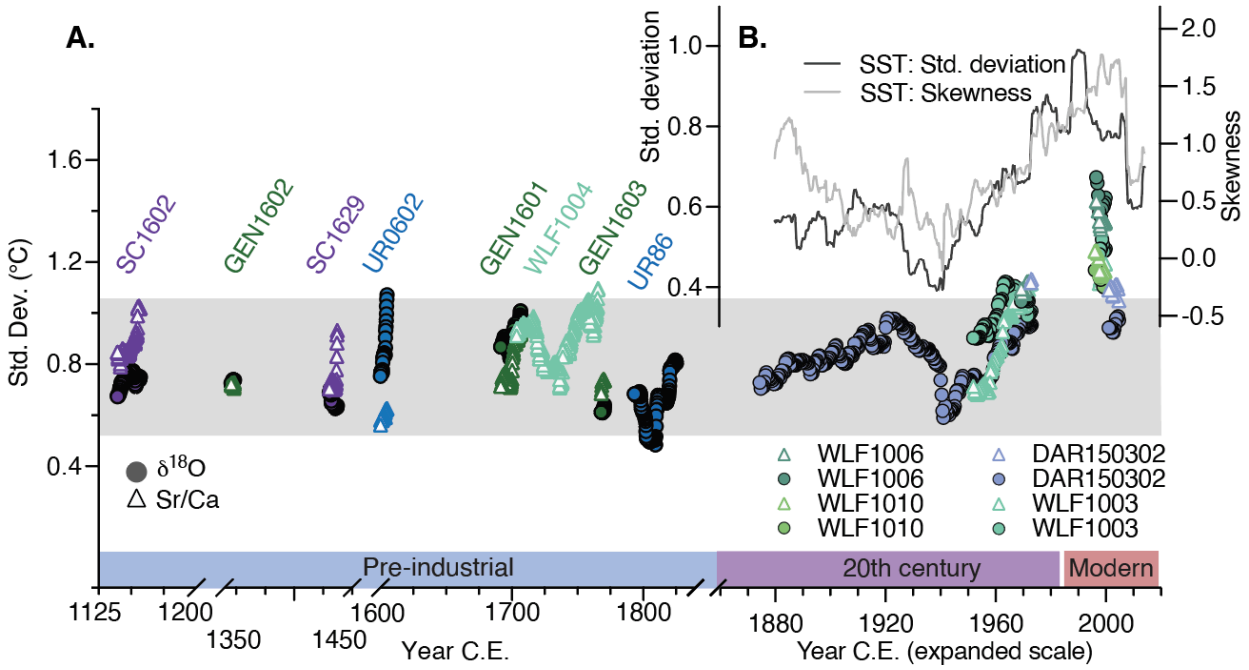

Figure 2. Variability of reconstructed EP SST compared with 20th century SST statistics. A. Colored symbols represent the 20-yr running standard deviation of interannual SST anomalies reconstructed from Galápagos corals, corrected for inter-island offsets. Circles represent coral $\delta^{18}O$-derived SST variability and triangles indicate SST variability derived from coral Sr/Ca. Time series lose 10 years off their start and end dates due to the 20-yr running calculation, and the gap centered in the1980's results from the death horizon in all modern Galápagos corals. Pre-industrial corals are labeled with sample IDs; post-1860 samples are identified in legend. **B.** Inset plot shows the 20-year running standard deviation for instrumental Galápagos SST in dark grey and the running 20-yr skewness of interannual anomalies in light grey (HadISST: 2°S-2°N, 88-92°W; (*61*). Shaded grey range indicates ±2s range (95% distribution) for pre-industrial variability. Shaded bars at bottom indicate preindustrial, 20th-century, and modern epochs. SST and coral data are processed as in Methods.

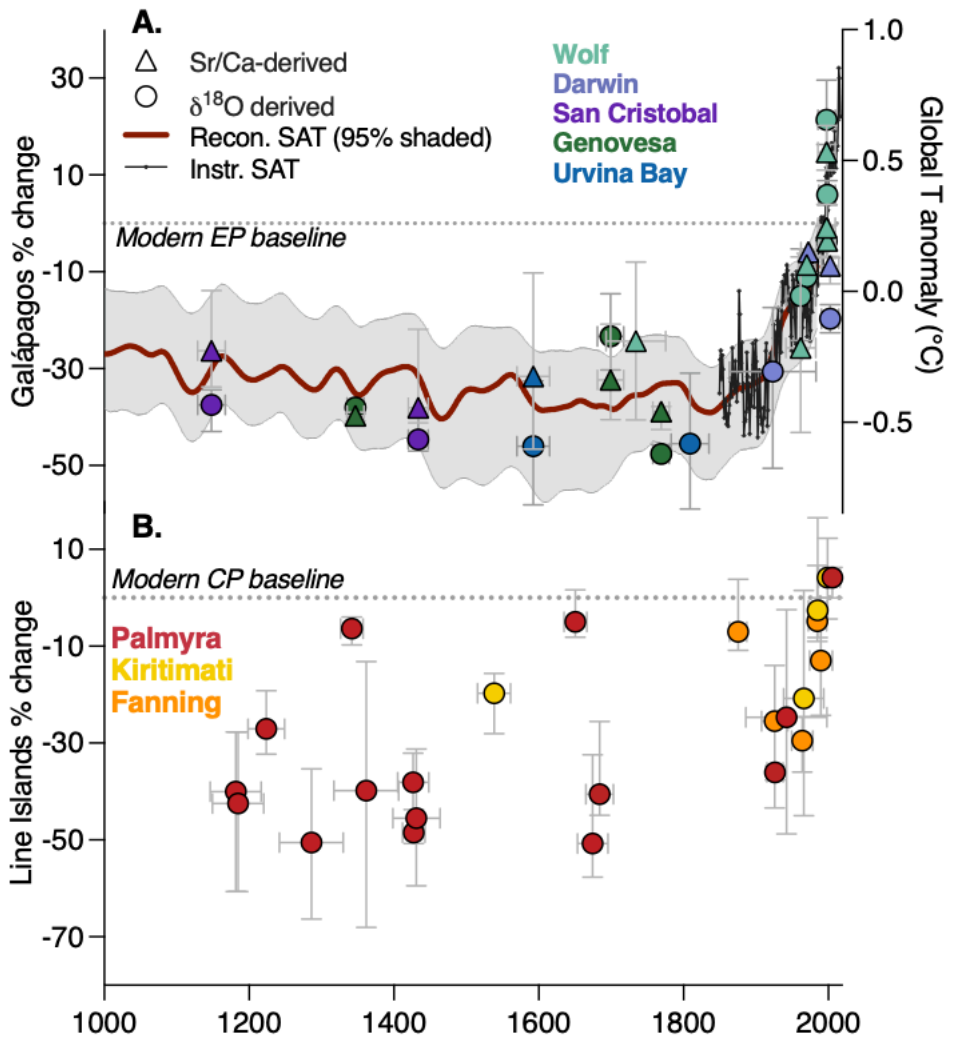

Figure 3. Comparison of interannnual variability in the tropical Pacific and global surface air temperature (SAT). A. Change in interannual SST variability from Galápagos corals, expressed as percentage change from modern. Each symbol represents a single record: colors represent different islands, and shapes indicate proxy type (circles: $\delta^{18}O$; triangles: Sr/Ca). Vertical and horizontal bars indicate ranges of percent change and ages, respectively. SAT change is indicated by black line (instrumental) and bold red line (reconstructed, with 95% confidence indicated by light grey shading) (*62, 63*). **B.** Change in interannual variability of coral $\delta^{18}O$ data from the northern Line Islands, expressed as percent change from modern as for A. Colors represent different islands as in legends.

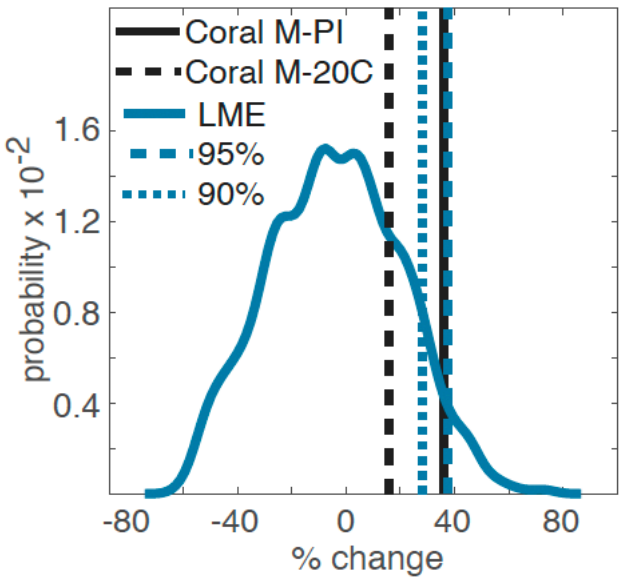

Figure 4. Distribution of percent change values simulated by the 11 fully forced members of the CESM1.2 LME ensemble, compared to Galápagos coral results. The solid teal line represents the distribution of percent change values for simulated SST anomalies at 120°W, calculated as described in Methods. The 95% distribution (two-tailed) is indicated by the teal dashed line (at 36%), and the teal dotted line represents the 90% level (28%). The solid black line indicates the reconstructed percent change in EP-ENSO SST variability from modern to pre-industrial (37%), and the black dashed line represents the coral-reconstructed weakening between modern and 20th century epochs (16%).

Table 1:
Percent change in variability between epochs for corals.

	Pre-industrial last millennium	**Post-industrial/ 20th century**
Interval	1000-1850 CE	1851-1982 CE
*% change from modern (post-1984)**		
Galápagos	37% (±8); p<0.00001	16% (±9); p<0.01
Line Islands	38% (±12); p<0.0001	17% (±17); p<0.05

*Calculated as (older – modern benchmark)/modern benchmark.
Benchmark intervals given in Table S5.

Supplementary Materials for

Recent intensification of eastern Pacific ENSO is unprecedented across the last millennium

J.E. Cole[1]*, D.M. Thompson[2], K.A. Dyez[1], C.J. Tripp[1], A.W. Tudhope[3], M. Lofverstrom[2], S. Stevenson[4], J.M. Okun[1], A.E. Lawman[5], J.L. Conroy[6], J.T. Overpeck[7], G. Jimenez[8], R.L. Edwards[9]

Corresponding author: colejul@umich.edu

The PDF file includes:

Materials and Methods
Supplementary Text
Figs. S1 to S14
Tables S1 to S7
References 60-80

Materials and Methods

This study includes 28 time series from 13 cores across 5 islands in the Galapagos (table S1). All of these are either being presented here for the first time, or have been updated from previously published data as described below.

Coral Sampling

This study includes cores from both living and subfossil coral colonies. All corals are *Porites lobata* except for UR86 (*Pavona clavus*; (*64*)). Living colonies were sampled at Darwin and Wolf Islands using diver-operated hydraulic or pneumatic drills. Subfossil colonies were sampled using gas-powered drills from shoreline deposits at 0-5m above sea level; one exception (Wolf10-04) was recovered from a submerged dead coral colony at ~12m depth, using the same methods as for living colonies (*65*). Cores were processed using standard methods: we rinsed them thoroughly and removed a slab from the middle of the core using a tile saw. In some cases, cores were scanned prior to slabbing using computerized tomography, which guided slab orientation. The remainder were slabbed using visual features as a guide, and the slabs were then X-rayed. The resulting density images were used to identify sampling transects along optimal pathways (defined by rapid upward growth, alignment with growth direction, and outward-fanning structures). We cleaned the slab ultrasonically with deionized water and used a "water-pick" to clean the sampling transect. We sampled the slabs at ~monthly (1mm) resolution using a computer-led micromill. (Wolf 10-06 was drilled at 0.5mm resolution in the post-1983 section due to a slightly slower growth rate.) We examined multiple scanning electron micrographs from each core to identify secondary aragonite or other nonprimary structures. Cores presented here exhibited well-preserved primary aragonite in their SEM images.

We use 14 records of $\delta^{18}O$ and 14 of Sr/Ca to produce this reconstruction of EP ENSO variability. Some of these have been previously published, and those records are described in the original references (Table S1). However, we have updated these as follows:

- Wolf10-04: we redrilled some of the sampling transects that were previously flagged as suboptimal (*65*), and we replaced data from the initial transects with data from the improved transects.
- Wolf 10-03: we discovered a sampling error in data prior to 1983 (*34*). We redrilled and reanalyzed all pre-1983 data and have replaced old data with new data.
- Wolf 10-10: a prior study generated only Sr/Ca data (*34*), and in some cases, original powders had been completely used; we therefore needed to redrill samples to generate a 1mm-resolution isotope record. In so doing, we found it appropriate to adjust the age model (by ≤1yr) in part of the record. (Note that isotope and Sr/Ca data are not always analyzed on the same powders as a result; online data for Wolf10-10 indicate where this is the case.)
- UR86: this is the sole case in which we used data published by another research group (*64*). We found it necessary to adjust this record: the original age model did not place $\delta^{18}O$ maxima in the cool season and minima in the warm season, because ages were assigned using annual density banding assumptions (*32*). We retained the absolute annual ages from the original publication, but redated the record internally so that the seasonal cycle corresponds to the typical Galápagos pattern.

Table S1 indicates where each record was produced. If no lab is indicated, see the original reference. For the unpublished records and the updates described above, nearly all samples were analyzed at the University of Michigan PACE lab: for $\delta^{18}O$ we used a Delta V isotope ratio mass spectrometer (IRMS) coupled to a Kiel 3 autosampler, and for Sr/Ca we used a Thermo ICAP Duo 7400 inductively coupled optical emission spectrometer (ICP-OES). Some of the records were analyzed at the University of Arizona: isotopes were run on a Finnigan MAT 252 with Kiel 3 autosampler in the Environmental Isotope Lab, and elements were analyzed on the same Thermo ICAP Duo 7400 ICP-OES in the Coral, Cave, and Climate Lab. Analytical uncertainties are as follows: UM-PACE $\delta^{18}O \pm 0.08‰$, based on an in-house standard (Luxor) calibrated to NBS-19. UA MAT-252 $\delta^{18}O \pm 0.10‰$, based on an in-house standard (Carrara) calibrated to NBS-19. All Sr/Ca ±0.02 mmol/mol based on an in-house standard (Mafia) calibrated by ICP-MS data measured at the University of Western Australia.

Age Models

Each core has one absolute age control point. Absolute ages for each subfossil colony derive from U/Th methods (*66*) (table S2). For cores from living colonies, known drilling dates provide an absolute age at the top. Within each core, subannual ages were assigned based on clear annual cycles in Sr/Ca and $\delta^{18}O$ (figs. S4-6). We assign annual Sr/Ca and $\delta^{18}O$ minima to the warmest month of March; we do not use the SST minimum (geochemical maxima) because the timing of peak upwelling varies widely across the year due to interannual ENSO variability (*65*). We interpolate between age tie points to calculate ages for each depth, and then interpolate each record to monthly resolution. Because some records had fewer than 12 samples/yr, we converted all records to bimonthly data by averaging Jan-Feb, Mar-April, etc.

Every core from a living colony in our Galápagos sample pool has a growth hiatus (death horizon) corresponding to the 1982-3 El Niño event: this heat extreme killed 95-99% of all corals in the main archipelago of the Galápagos (*67*), but the corals at Wolf and Darwin regrew (*68*). We therefore have multi-year gaps in all modern records, ranging from 3-9 years, and none of our modern time series preserve this event fully. In these cores, we assigned ages below the hiatus by aligning the geochemical data with instrumental SST, assuming the hiatus begins around 1982; distinctive variations in SST and geochemistry made this process straightforward. We treat the core above and below the hiatus as different records.

Because the data lack coverage of the 1982-3 extreme El Niño event, and the strong 2015-6 and 2023-4 events that occurred after sampling, our estimates of modern variability are conservative.

Geochemistry-SST calibration

To directly compare $\delta^{18}O$ and Sr/Ca data, we converted each record to SST using locally derived calibrations of $\delta^{18}O$ (-0.165‰ per °C) and Sr/Ca (-0.0597 mmol/mol per °C). We derive these slopes using weighted least squares analysis (*69*) from monthly Sr/Ca and $\delta^{18}O$ in the modern cores (WLF10-03, WLF 10-06, WLF10-10, and DAR15-03-02) and local SST from OISSTv2 (0.25° grid) (*60*). In addition, we used published coral $\delta^{18}O$ and logger SST data (*70*) to obtain a single mean slope from that study. The final Sr/Ca calibration slope represents the mean of the 4

modern coral calibrations, and the final $\delta^{18}O$ slope reflects the mean from the 4 corals and the single value from Wellington, Dunbar and Merlen (*70*). We explored an alternate approach using annual (April-March) mean values of geochemical and instrumental data; this yielded steeper slopes of -0.219 ‰ per °C and -0.073 mmol/mol per °C, but the uncertainty on the interannual slopes is larger (table S3). We use the monthly calibration. Because we characterize variability change with a metric of change relative to modern, our % change results are not sensitive to calibration slopes.

Calculating the interannual variability of SST

To obtain a measure of SST variability from each record, we used bimonthly reconstructed SST calculated using the monthly SST calibration. From each bimonthly record, we removed the mean seasonal cycle, high-pass filtered the data at 10 yrs, and smoothed the resulting record at 6 months to isolate the interannual signal. We then calculated a 20-yr running standard deviation, incremented by 2-month steps, and use the mean, minimum, and maximum to define the 20-yr variability and its range for each core. These methods are similar to those used in previous work (*29, 30*). We calculate skewness (total and running 20-yr values) on the same filtered, bimonthly data used for the running standard deviation (fig. S8, S9).

Geographic correction factor

In the Galápagos, upwelling of cool water that peaks in August-September drives a strong seasonal SST cycle, and the influence of this upwelling varies systematically across the archipelago, creating a gradient in both mean SST and interannual variability (figs. S1, S7). On interannual time scales, upwelling and advective changes further impact SST, with reduced upwelling, deeper thermocline, and warmer SST during El Niño years. Thus the variability of SST anomalies differs among the islands, by up to 15%, with stronger variance in the central archipelago (particularly the west and south) due to the influence of equatorial upwelling and the shoaling of the eastward equatorial undercurrent against the Galapagos platform. Because these features are equatorially confined, colder waters will always be more influential in the equatorial and western sites. To correct for this background gradient and provide a basis to compare results across islands, we used the OISSTv2 dataset of 0.25° gridded SST anomaly to quantify the SST variability at each site and derive a correction factor (table S3; fig. S7). We scale the 20-yr standard deviations from all islands to that observed at the northeast end of San Cristobal island (this choice is arbitrary). Figure S10 compares our results with and without this correction.

Percent change metric

We define a % change metric to compare the variability among the Galápagos coral records and across datasets, similar to previous studies (*28, 29*). We use the standard deviation from the filtered bimonthly anomalies over the 20-yr interval of approximately l990-2010 as a modern benchmark for comparison with earlier intervals. Between-core differences in the actual benchmark interval used are small and unavoidable due to different core lengths (Table S5). We calculate %change as ((older – benchmark)/benchmark) where “benchmark” is the standard deviation over the 20yr benchmark interval and older is the standard deviation value for any given core. This tells us “how much weaker was the variability in the past?” We distinguish

between the benchmark interval (1990-2010) and the modern epoch in our records. The latter varies by core and is defined as all data above the 1982-3 death horizon.

Comparison with central Pacific corals

For comparison with the Galápagos records, we use published coral records from the northern Line Islands (central Pacific). Our methods differ somewhat from previous analyses of these data (*29*). We selected all $\delta^{18}O$ records from individual coral colonies of at least 20 years from Palmyra, Kiritimati, and Fanning Islands available on the NOAA Paleoclimatology database (https://www.ncei.noaa.gov/products/paleoclimatology; table S6). Where composite records had been constructed, we used only the individual cores and not the composite. We converted all data to bimonthly resolution, removed the seasonal cycle, and high-pass filtered the data at 10 years, as for Galápagos records. Due to the contribution of seawater $\delta^{18}O$ to the coral signal in the central Pacific, and following the lead of original authors, we did not convert $\delta^{18}O$ values to SST.

We account for inter-island differences in climate signals in our percent change calculation: for the Line Islands, we computed the percent change in variance from modern by comparing each record to a modern record from the same island, rather than taking a regional average of modern records. Furthermore, we used only the post-1984 interval to define the modern, to be consistent with the Galápagos cores that are missing the 1982-3 El Nino event. Finally, we excluded cores <20 years in length. This procedure left us with a single modern core from each of the three northern Line Islands for the modern comparison. Because of the different time spans covered by these cores, the modern benchmark period is slightly different for each island. We chose 20-yr intervals for each island that include a single strong event, as the Galápagos interval does (Table S5).

We explored epochal differences in the Line Islands by splitting the data into the same epochs as for Galápagos, to facilitate comparison: pre-1850 (pre-industrial); 1850-1982 (20^{th} century), and post-1984 (modern). For this comparison of epochal means, we removed Line Islands records that, once split into these intervals, were less than 20 years long. To calculate changes from modern, we again compared pre-industrial and 20^{th}-century coral data with modern data from the same island to account for inter-island differences in variance.

Comparison with other fossil coral datasets:

Coral datasets from the southwest Pacific (Vanuatu Sr/Ca) and eastern Indian ocean (Mentawai $\delta^{18}O$) have been similarly used to address last-millennium changes in tropical variance (*30, 46*). Using the same methods as applied to Galápagos records, we find trends towards higher variability, in agreement with the original studies (fig. S11). Neither site shows the distinct separation between modern and preindustrial variability that we see at Galápagos. A wide range of preindustrial variability in the Mentawai data is consistent with both the influence of seawater $\delta^{18}O$ on coral records and the strength of the Indian Ocean Dipole, an important driver of variance at Mentawai that is not strictly controlled by ENSO. At Vanuatu, the range of SST variance is small compared to the eastern equatorial Pacific, and the small number of cores prevents detailed analysis of the transition across the past millennium..

Comparison with continuous ENSO reconstructions:

We analyze several continuous ENSO reconstructions that use either multiproxy (*42*), coral-only (*14*), or tree-ring-only (*43*) records from ENSO-sensitive regions. The multiproxy study uses proxy data within 35° of the equator that has a temporal resolution and age model uncertainty of ≤5yrs and extends beyond 1851-1974; three different SST datasets were used to provide Niño 3.4 reconstruction targets. The multiproxy study draws on both coral and tree-ring data that also inform the others. The coral study uses a network of 27 Indo-Pacific coral records to reconstruct both CP and EP (termed warm pool, WP, and cool-tongue, CT, respectively) time series at seasonal (4/yr) resolution. The tree-ring ENSO reconstruction, at annual resolution, is the first principal component of climate reconstructions from seven ENSO-sensitive regions. These and other similar studies draw on many of the same paleoclimate datasets across the tropics, differing mainly in the methods and reconstruction targets used.

To compare with the Galápagos results, we processed these reconstructions in the same way, and calculated the running 20-yr standard deviation on filtered anomalies. Only the Freund et al. (2019) product has subannual resolution (4/yr); we removed the annual cycle and smoothed the data with a 2-point (6 month) running mean. The others are annually resolved and we applied no additional smoothing. All of these reconstructions show an increase in ENSO variability in the mid (WP) to late (all others) 19th century (fig. S12). Other multisite reconstructions, not analyzed here (but based largely on the same underlying datasets) agree with this late-19th century pattern. We suggest this pattern results from the age and data inhomogeneity biases discussed in the text. None show the sharp rise in the late 20th century that characterizes the Galápagos data.

Comparison with simulated last-millennium climate

To compare with Earth system model output, we use an ensemble of 11 fully forced simulations of the last millennium (the Last Millennium Ensemble, or LME, 850-1850) (*12, 45*). The underlying model CESM1.2, like many, has a known bias in too-strong trade winds that displaces ENSO SST fingerprints westward. We therefore used equatorial SST from 120°W to represent the EP SST mode; previous work has accounted for this bias similarly (*12, 71*). For reference, the equatorial longitude of the EP anomaly in a similar generation of CESM was identified as 118.25°W (*15*).

Our analysis used only the years that overlap with the coral data, to account for the influence of forcing. Simulated SST from each fully forced LME simulation was analyzed in the same way as the Galápagos coral data to yield the filtered bimonthly SST anomalies. We calculate the running 20-yr standard deviations for each simulation, and compare the standard deviation of each 20-yr interval with the average of that from all possible 20-yr intervals to provide a probability distribution of the percent change across all ensemble members (fig. 4). We calculate the 95% significance as a 2-tailed test to compare intensification reconstructed from the corals with that simulated by the model. We analyzed the control run similarly to produce fig. S13.

To visualize the simulated variability of ENSO from the last millennium through the 21st century, we used the 4 LME simulations that extend from 850-2100 CE (*45*). These were driven

by the full suite of forcings from the LME through 2005, and by RCP8.5 from 2005-2100. For each simulation, we calculated the percent change metric as above, and identified the 95% distribution from the preindustrial control (table S7), and for each individual ensemble (fig. S14). The time series of the running percent change values illustrates that the model tends to produce values above the 95% level more frequently in the 21st century, compared to the previous period, but the modern and projected %change does not emerge from the preindustrial background. Values exceeding 95% occur in all simulations prior to anthropogenic forcing. These pre-industrial strong intervals are short-lived and not coincident across the 4 simulations. Although a full analysis of these data is beyond the scope of this paper, and the number of ensemble members is insufficient to fully separate forced and internal variance, the contrast between the Galápagos results and the simulated trajectories of ENSO variability point to limitations in the LME simulation of ENSO, as discussed in the text.

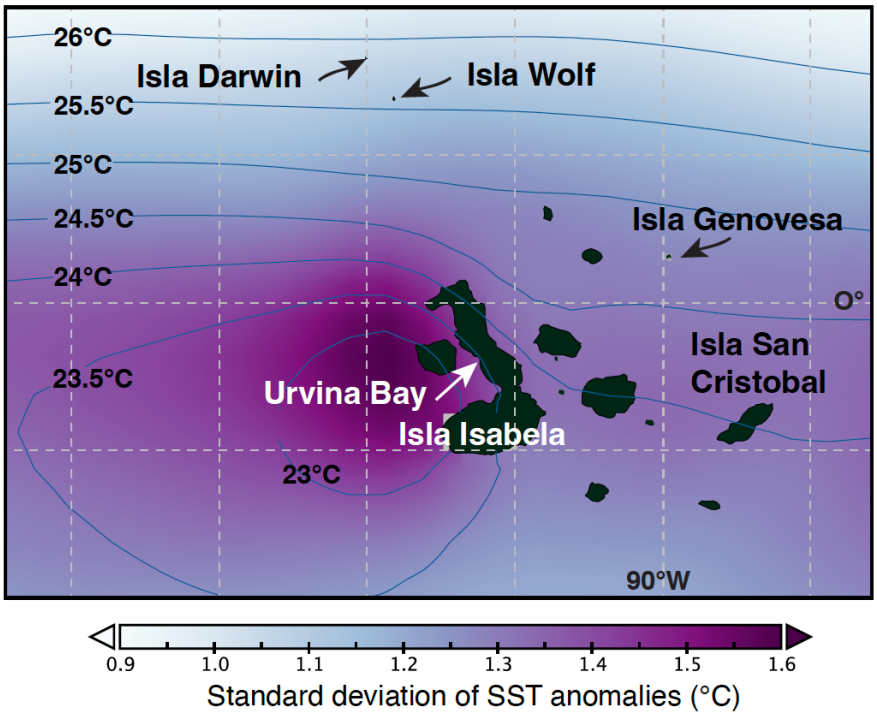

Figure S1. Map of the Galápagos islands showing coral sites and SST climatology across the archipelago. Contours indicate mean SST, and colors display the standard deviation of SST anomalies (1982-2024, using 0.25° resolution OISST product (*60*) accessed from https://climexp.knmi.nl/). Only islands with coral records are labeled. Grid spacing is 1° latitude and longitude; the equator and 90°W are labeled.

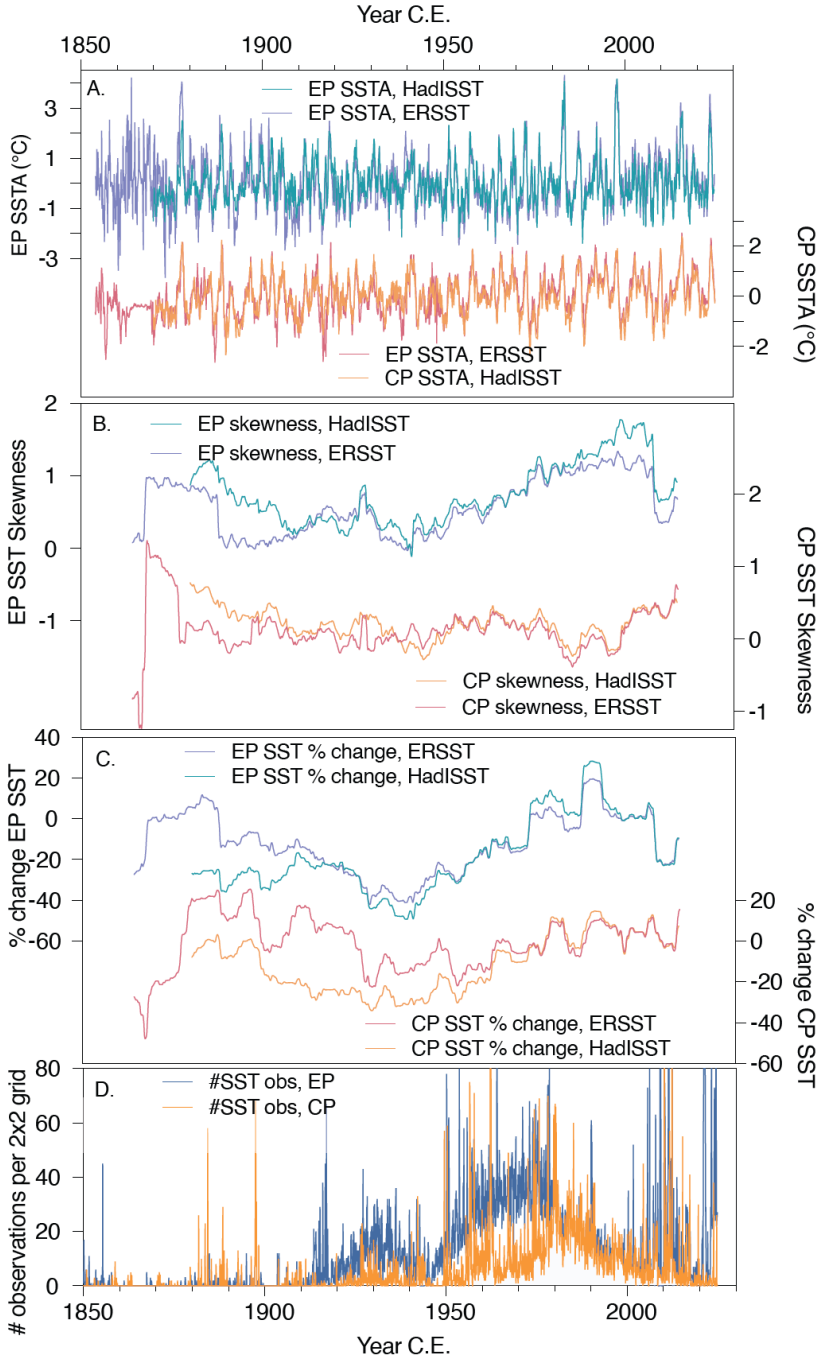

Figure S2. Comparison of instrumental SST data from different sources in the central (CP) and eastern Pacific (EP). HadISSTv1 (*61*) and ERSSTv5 SST data (*72*) are shown for the regions around Galápagos (EP; blue/green colors) and the northern Line Island (CP; red/orange colors) since 1850. **A.** Monthly SST anomaly. **B.** Skewness of SST data, with positive skewness denoting stronger warm events. **C.** Percent change from modern interannual variability over 20-year periods, calculated as in methods for coral data. **D.** Number of SST observations per 2° x 2° grid square in the iCOADS historical SST dataset, which informs the ERSST and HadISST products. "EP" data represent the Galápagos region, 2°S-2°N, 88°-92°W. "CP" data represent the northern Line Islands region, 2°-6°N.

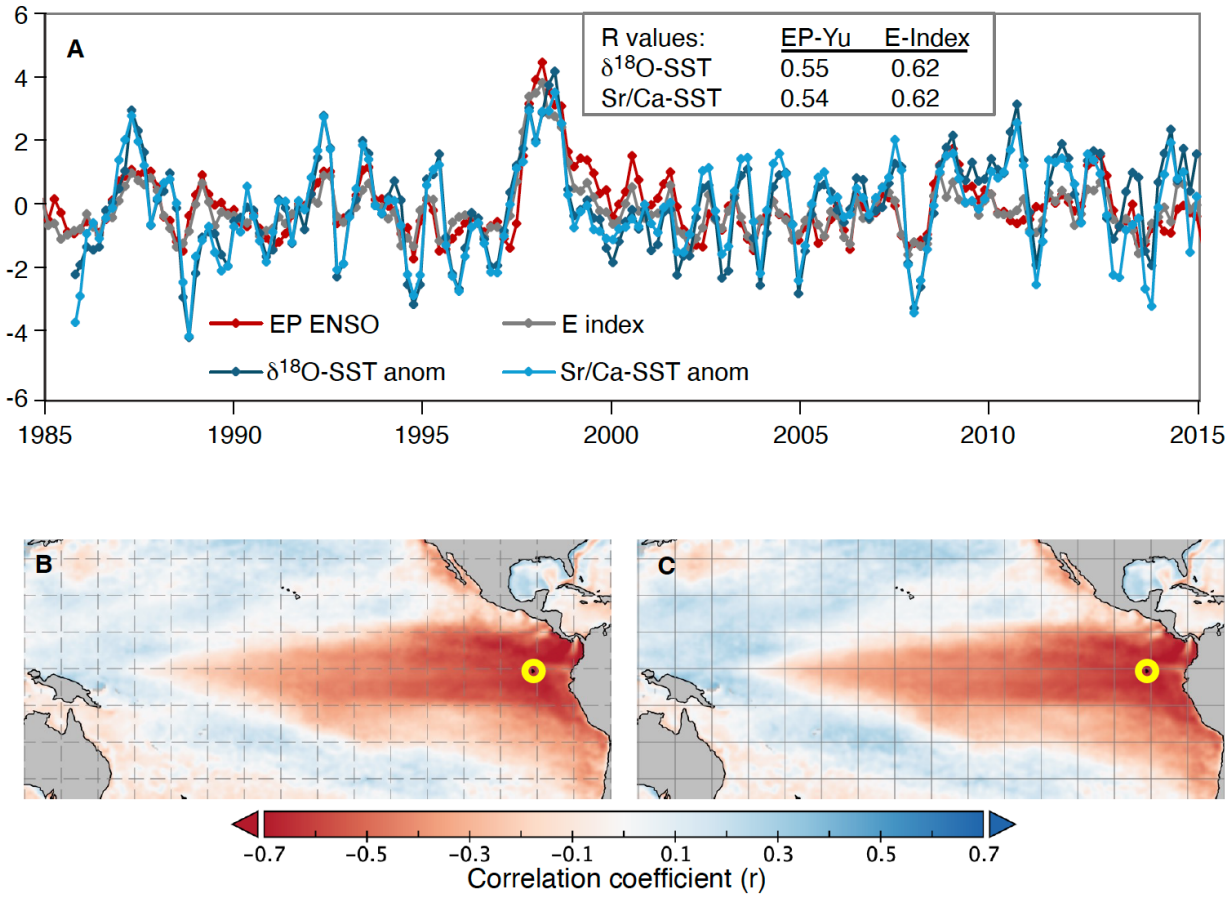

Figure S3. Comparison of Galápagos coral geochemical anomalies with large-scale indices of eastern Pacific ENSO variability. A) EP-ENSO index (red; (*19*); https://www.ess.uci.edu/~yu/2OSC) and E-index (grey (*11*)), compared with mean SST anomalies from Sr/Ca and $\delta^{18}O$ (light and dark blue) in 4 cores that grew at Wolf and Darwin islands. E-index is calculated as: E = Nino1+2 – (0.5*Niño4) after (*11*). Correlations are significant at >99%; for comparison, these indices correlate with local (Wolf) SST at r = 0.68 and 0.81, respectively. Coral units are °C; EP index units are standardized. **B)** Map of correlation between coral $\delta^{18}O$ and SST anomaly at bimonthly resolution. **C)** Map of correlation between coral Sr/Ca and SST anomaly at bimonthly resolution. All SST anomaly data are 0.25° resolution from OISSTv2 (*60*), updated from https://climexp.knmi.nl/. Coral data are the mean of modern (post-1983) anomalies from four corals. Maps are very similar because mean Sr/Ca and $\delta^{18}O$ are highly correlated (r = 0.93).

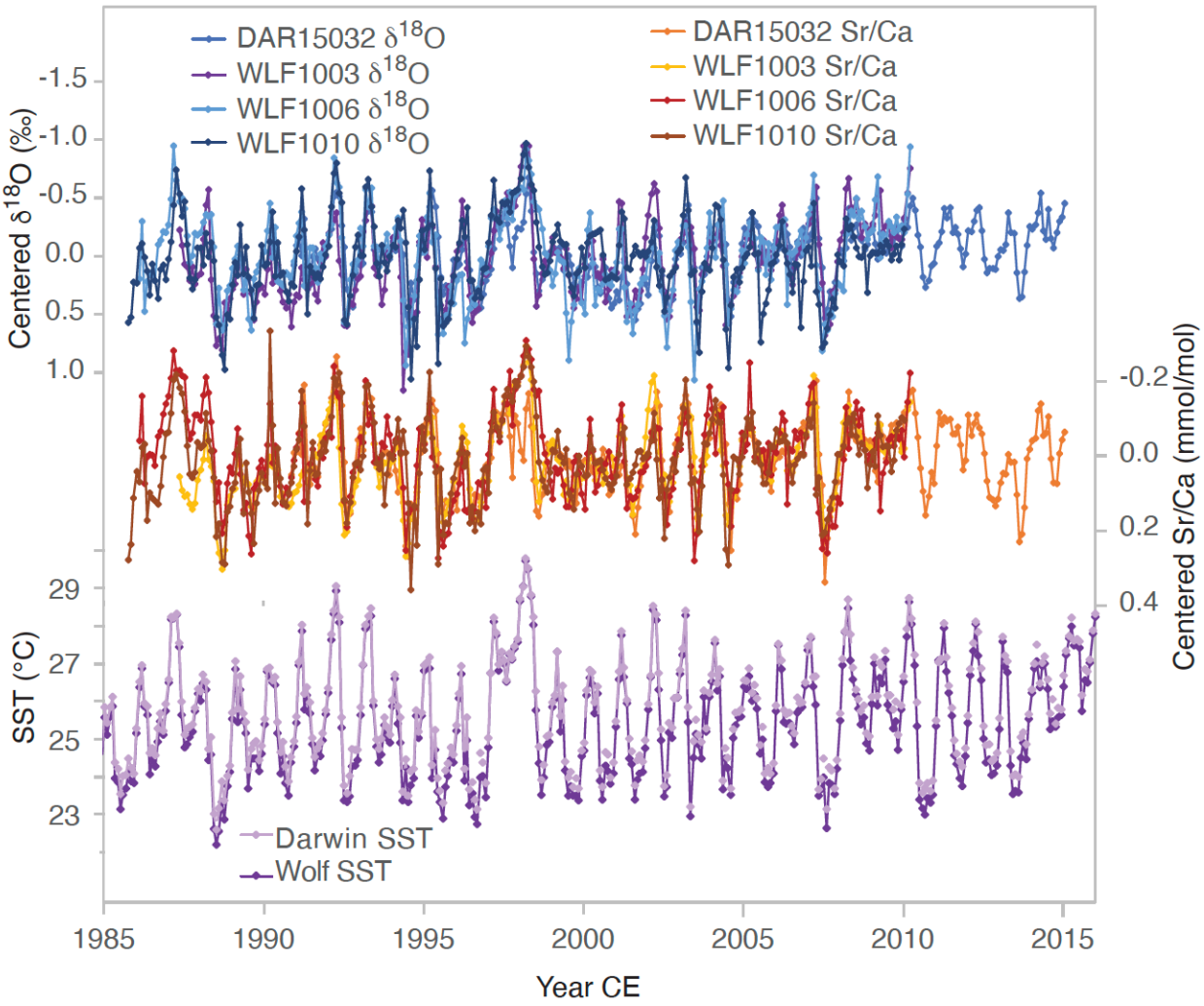

Figure S4. Modern coral $\delta^{18}O$ and Sr/Ca from 4 cores at Wolf and Darwin Islands, compared to instrumental SST. For all coral data, the mean of the common interval (1990.875-2010.208) has been removed to facilitate plotting. Correlation coefficients between coral and SST data range between -0.63 and -0.78, using only one age model tie point per year. SST data is from OISSTv2 (*60*).

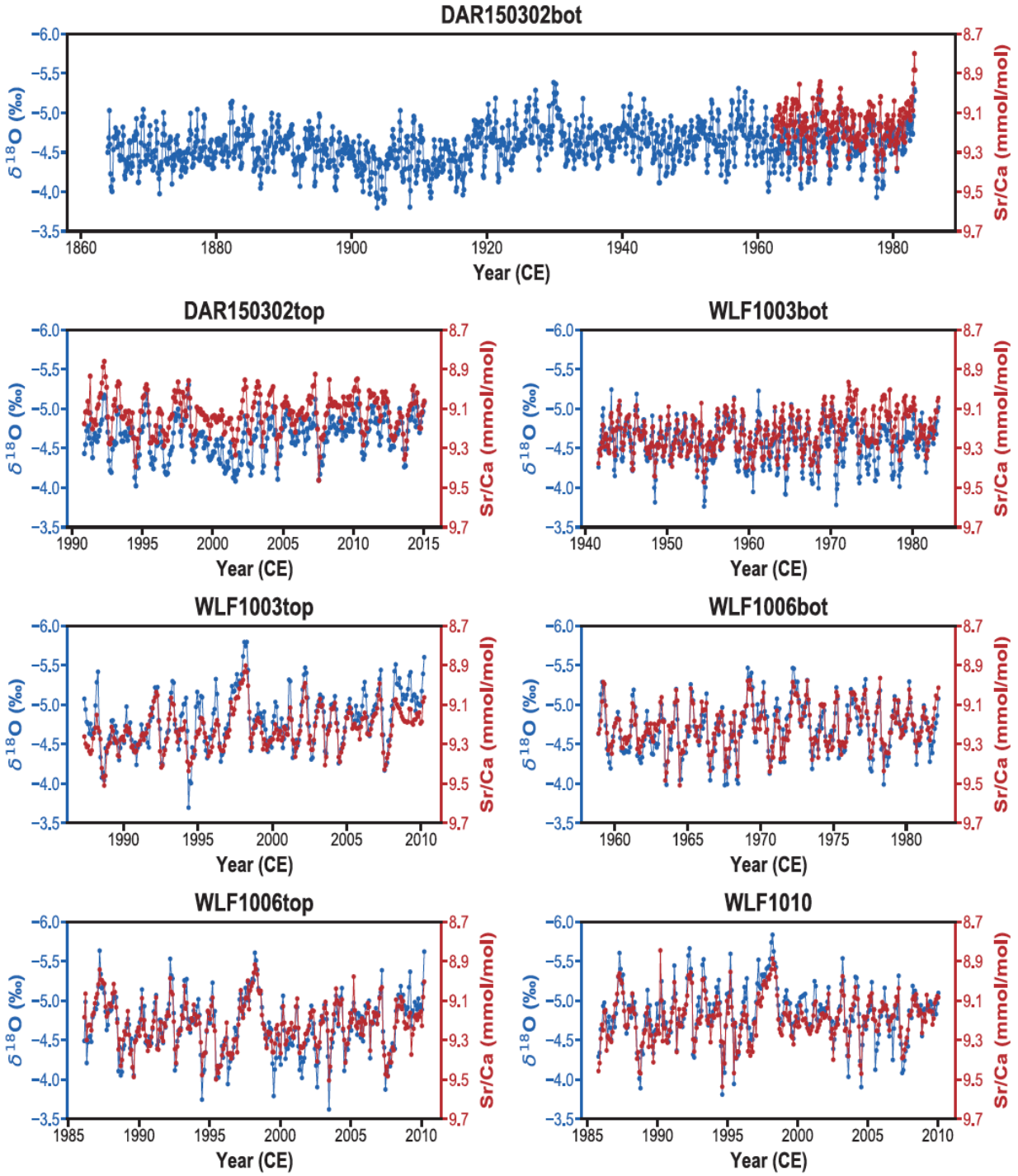

Figure S5. Galapagos coral $\delta^{18}O$ (blue) and Sr/Ca (red) data from the modern and 20th-century epochs since 1850. Data have been interpolated to bimonthly resolution. Site codes are listed in Table S1.

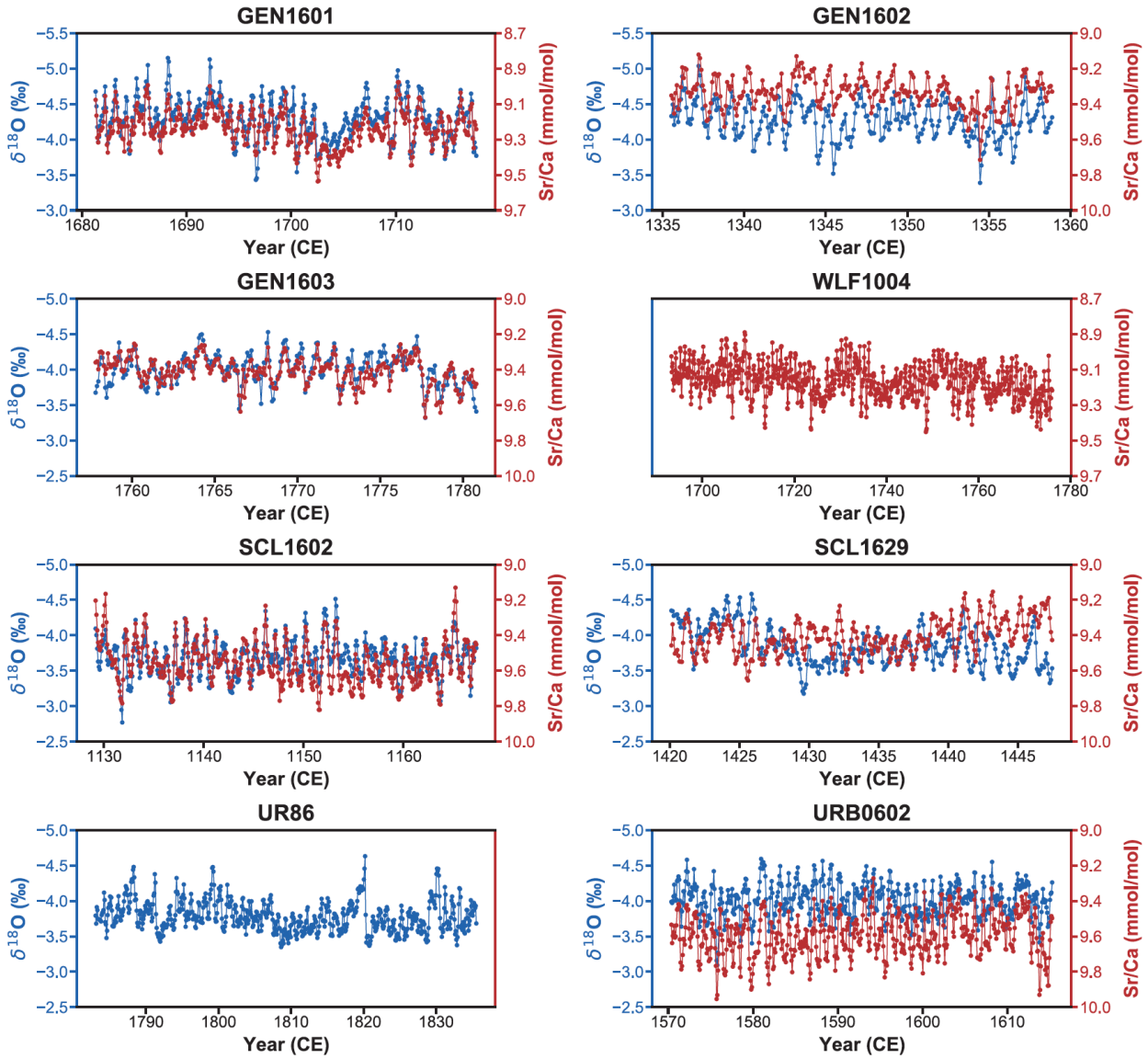

Figure S6. Galapagos coral δ^{18}O (blue) and Sr/Ca (red) data from the pre-industrial epoch, before 1850. Data have been interpolated to bimonthly resolution. Site codes are listed in Table S1.

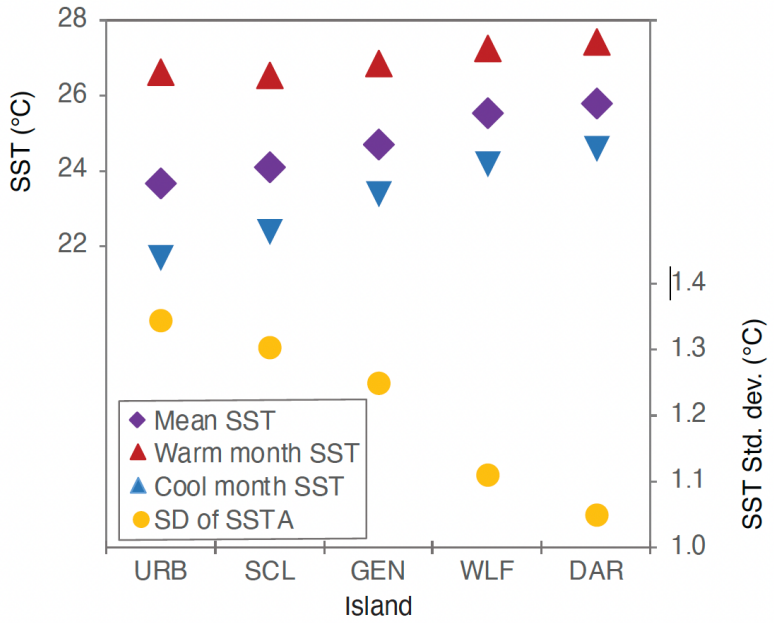

Figure S7. Inter-island variability in SST characteristics across the Galápagos archipelago. Top: mean SST (purple diamonds) flanked by warm month and cold month values (red and blue triangles). Bottom: Yellow circles denote the standard deviation of SST anomalies (i.e. seasonality removed), September 1981-October 2021. OISSTv2 (*60*) observations, anomalies, and seasonal values accessed on KNMI Climate Explorer (https://climexp.knmi.nl/start.cgi). Islands: URB = Urvina Bay, Isabela; SCL = San Cristobal; GEN = Genovesa; WLF = Wolf; DAR = Darwin.

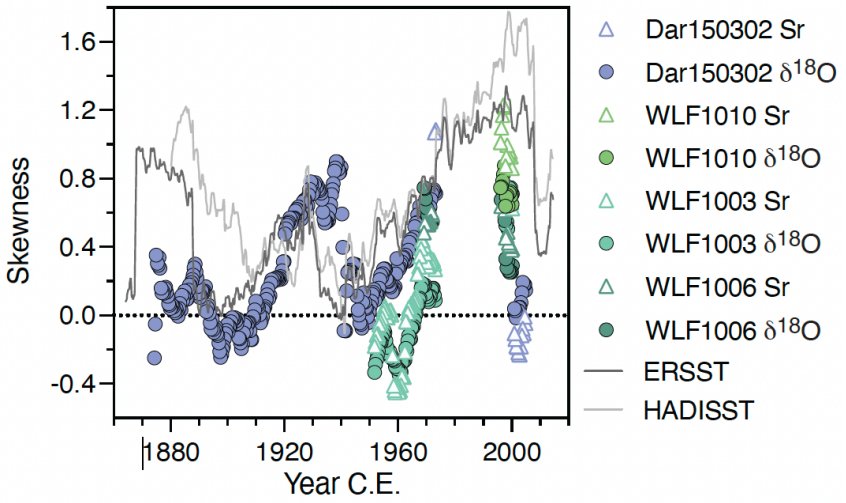

Figure S8. Comparison of running 20-yr skewness among coral and instrumental SST data. Grey lines indicate skewness calculated from the ERSST (darker line) and HadISST (lighter line) products (*61, 72*). Colored symbols indicate skewness calculated from coral $\delta^{18}O$ (circles) and Sr/Ca (triangles) data. All skewness values are computed as 20-year running values on the time series of smoothed, filtered SST anomaly data, at bimonthly resolution. These are the same data that were used for the 20-yr running standard deviation metric indicating variability.

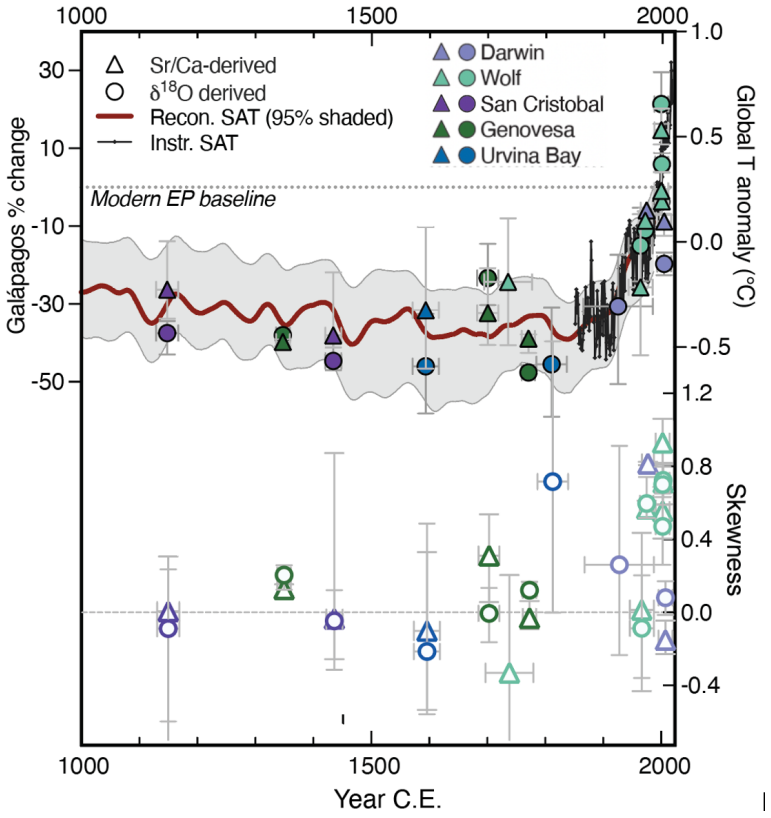

Figure S9. Comparison of variability and skewness from Galápagos coral data. A. EP-ENSO variability as in fig. 2. **B.** Skewness of SST anomalies, shown with open symbols using the same color scheme as in A, and calculated on the same filtered SST anomaly data used for the running standard deviation metric. Vertical bars indicate minimum and maximum 20-yr running values, and horizontal bars reflect the total length of each coral record.

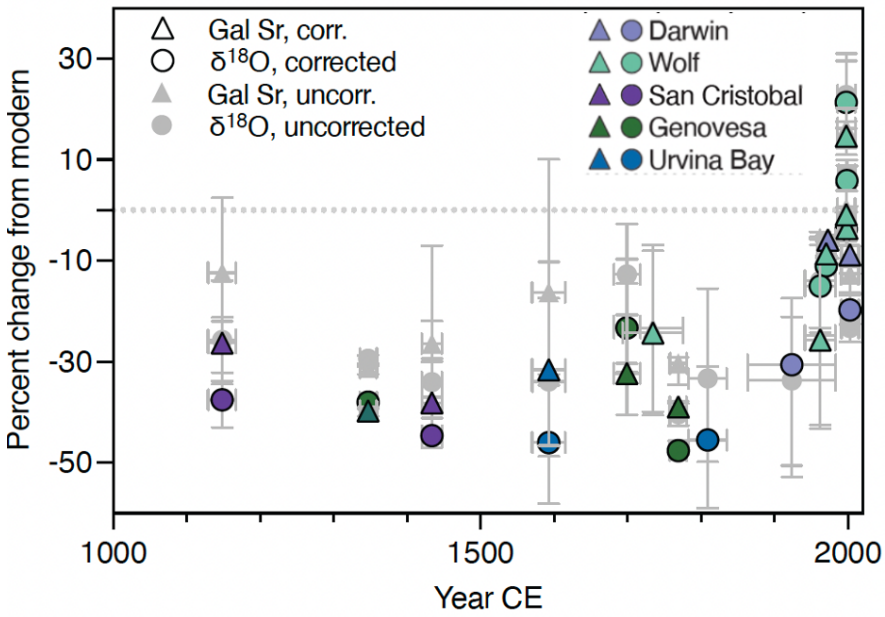

Figure S10. Comparison of reconstructed variability with and without a geographic correction. Data in colored symbols are reconstructed variability as in fig. 2, with sites indicated by colors and proxy by shape. Grey symbols represent the same data uncorrected for geographic differences in variability.

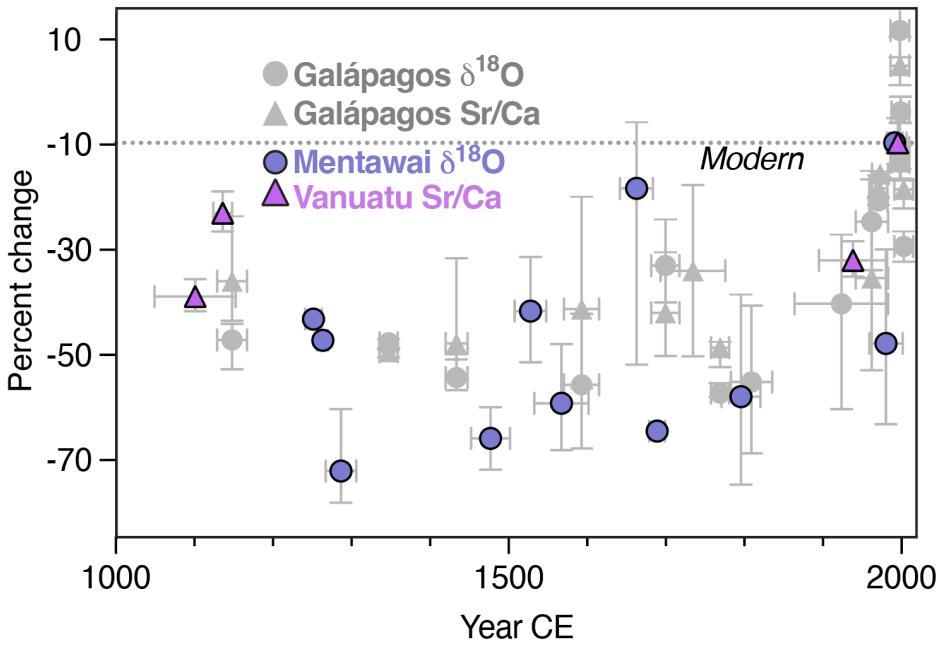

Figure S11. Percent change in interannual variance at Mentawai (red) and Vanuatu (gold), compared with Galápagos. Data from Mentawai (Sumatra, Indonesia (*46*))and Vanuatu (*30*) were processed as for Galápagos to remove seasonality, long-term variations, and noise (Methods). Percent change in interannual variance was calculated by comparison to modern samples from those sites.

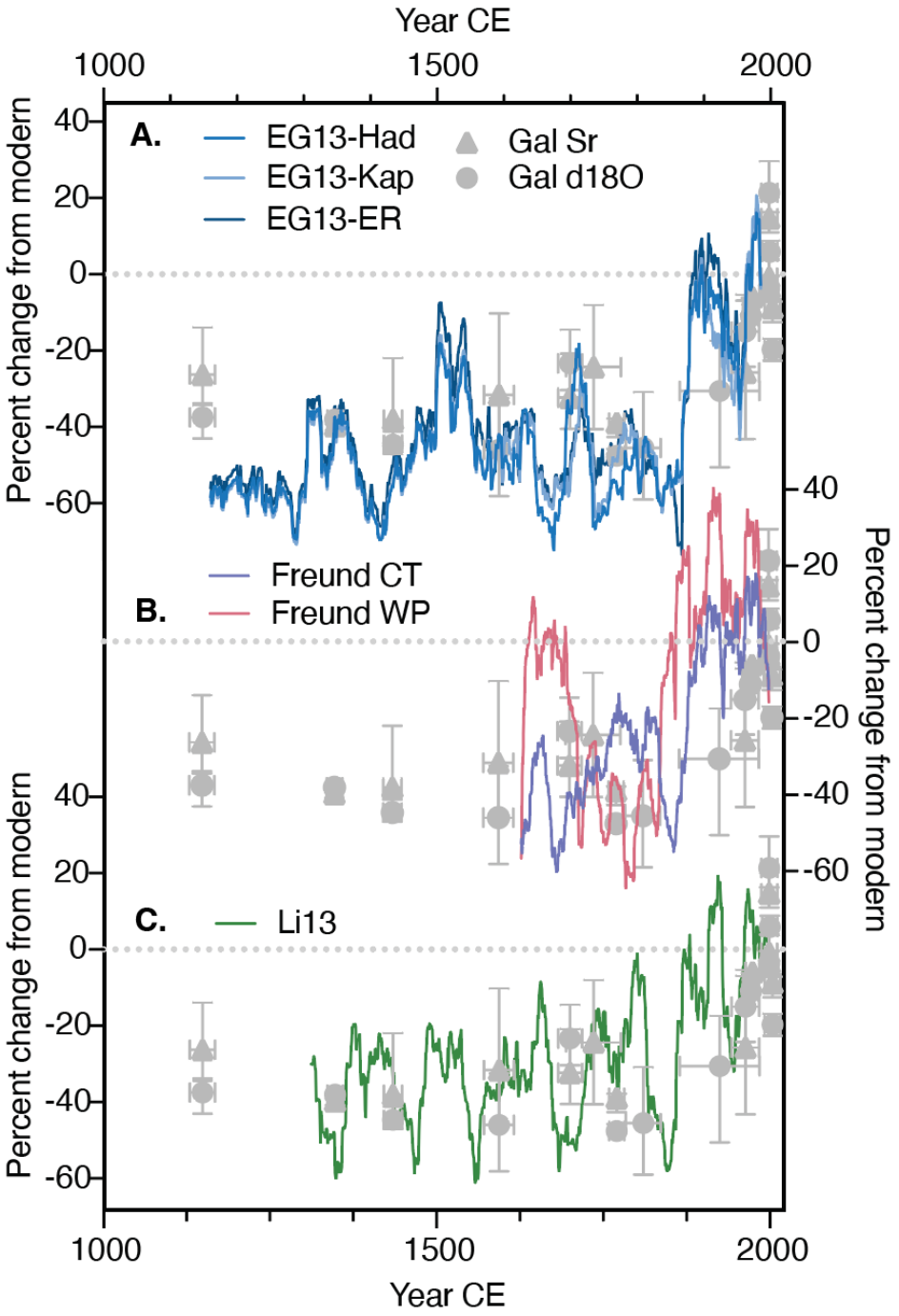

Figure S12. Last millennium ENSO variability in Galápagos coral compared to multi-site reconstructions. In all panels, the grey symbols represent the Galápagos data from fig. 2, and the colored lines show the same variability metric (percent change from modern) calculated for continuous ENSO reconstructions derived from multiple sites. **A.** Blue lines represent variability in Niño 3.4 SST reconstructed using HadISST2i, ESRSSTv3, and Kaplan SST datasets as targets (*42*). **B.** Variability is shown from seasonal reconstructions of the warm-pool (red) and cool tongue (purple) ENSO variability based on Pacific corals (*14*). **C.** Green line indicates variability calculated from the Niño3.4 SST reconstruction based on a global network of tree-ring sites (*43*).

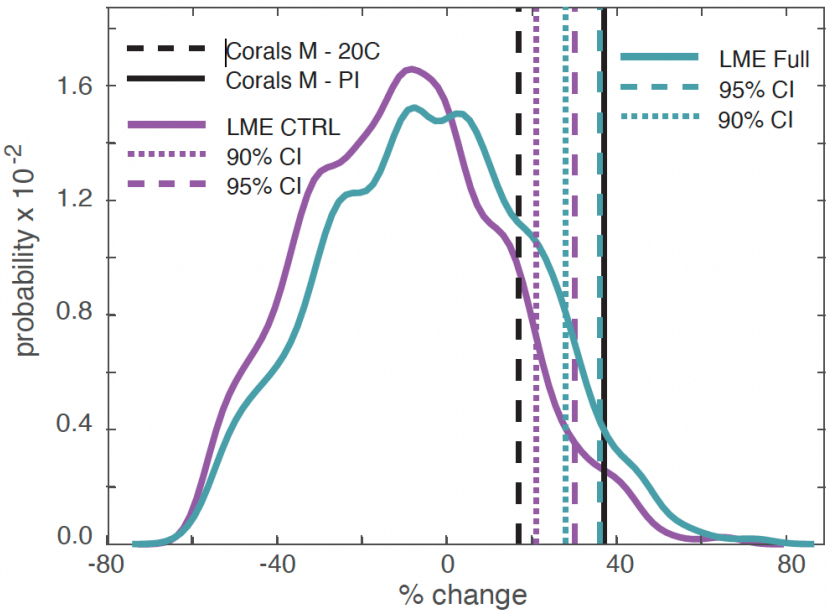

Figure S13. Distribution of simulated percent change values in forced and unforced simulations, compared to Galápagos coral results. The purple line represents the distribution of percent change values for simulated SST anomalies at 120°W, calculated as described in the Methods and using the unforced control simulation. The 95% significance level (two-tailed) is indicated by the purple dashed line, and the purple dotted line represents the 90% level. The solid black line indicates the 37% increase in variance reconstructed from Galápagos corals from modern (1990-2010) relative to pre-industrial (pre-1850). The black dashed line represents the 16% increase from the ~20th century interval (1851-1982) to modern (1990-2010). For comparison, the aqua line represents the distribution of percent change values calculated for the fully forced members of the LME ensemble (*45*), with the 90 and 95% levels in dashed aqua, reproduced from figure 4.

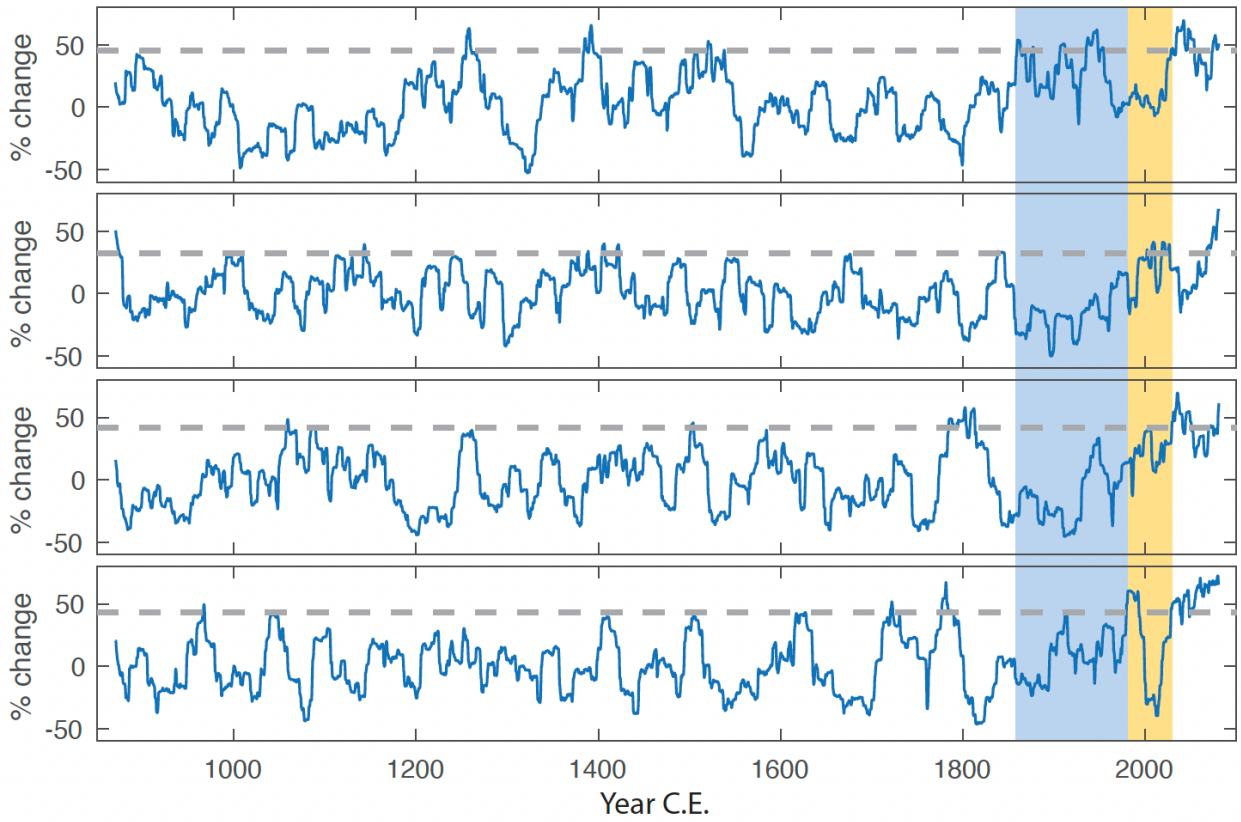

Figure S14. Simulated change in eastern Pacific SST variability in the four fully-forced members of the LME that extend to 2100. Model simulations were forced with the full suite of natural and anthropogenic forcings through 2005 and extended to 2100 using the RCP8.5 scenario (*45*). Percent change is calculated as the difference between the running 20-yr standard deviation of high-pass filtered SST anomalies compared to the average such value for the preindustrial control (Methods). The dashed line represents the 95% distribution level calculated using the preindustrial period; these differ slightly among ensemble members. Blue and yellow shading indicate the epochs used for coral comparisons (20th-century and modern, respectively).

Table S1. Galápagos core details

Core	Island*	Location	Proxy	Lab[@]	Years[$]	Reference
DAR150302top	DAR	1°40.63'N, 92°0'W	$\delta^{18}O$	UM	1990-2015	This paper
DAR150302top	DAR	1°40.63'N, 92°0'W	Sr/Ca	UA	1990-2015	This paper
WLF1010	WLF	1°23.15'N, 91°48.90'W	Sr/Ca		1985-2010	(*34*)[#]
WLF1010	WLF	1°23.15'N, 91°48.90'W	$\delta^{18}O$	UM	1985-2010	This paper
WLF1003top	WLF	1° 23.26' N, 91° 49.01' W	Sr/Ca		1987-2010	(*34*)[#]
WLF1003top	WLF	1° 23.26' N, 91° 49.01' W	$\delta^{18}O$	UM	1987-2010	This paper
WLF1006top	WLF	1° 23.26' N , 91° 49.01' W	$\delta^{18}O$	UM	1986-2010	This paper
WLF1006top	WLF	1° 23.26' N , 91° 49.01' W	Sr/Ca	UM	1986-2010	This paper
DAR150302bot	DAR	1°40.63'N, 92°0'W	Sr/Ca	UA	1962-1983	This paper
DAR150302bot	DAR	1°40.63'N, 92°0'W	$\delta^{18}O$	UA	1863-1983	This paper
WLF1003bot	WLF	1° 23.26' N , 91° 49.01' W	$\delta^{18}O$	UM	1941-1983	This paper
WLF1003bot	WLF	1° 23.26' N , 91° 49.01' W	Sr/Ca	UM	1941-1983	(*34*)[#]
WLF1006bot	WLF	1° 23.26' N , 91° 49.01' W	$\delta^{18}O$	UM	1958-1982	This paper
WLF1006bot	WLF	1° 23.26' N , 91° 49.01' W	Sr/Ca	UM	1958-1982	This paper
UR86	URB	0°15'S, 91°22'W	$\delta^{18}O$		1783-1835	(*64*)[#]
GEN1603	GEN	00°19.10'N, 89°56.94'W	$\delta^{18}O$	UM	1757-1780	This paper
GEN1603	GEN	00°19.10'N, 89°56.94'W	Sr/Ca	UM	1757-1780	This paper
WLF1004	WLF	1°23.27'N, 91°49.01'W	Sr/Ca	UA + UM	1693-1775	(*65*)[#]
GEN1601	GEN	00°19.10'N, 89°56.94'W	$\delta^{18}O$	UM	1679-1715	This paper
GEN1601	GEN	00°19.10'N, 89°56.94'W	Sr/Ca	UM	1679-1715	This paper
URB0602	URB	00°23.61'S, 91°13.98'W	$\delta^{18}O$	UM	1570-1615	This paper
URB0602	URB	00°23.61'S, 91°13.98'W	Sr/Ca	UM	1570-1615	This paper
GEN1602	GEN	00°19.10'N, 89°56.94'W	$\delta^{18}O$	UM	1332-1359	This paper
GEN1602	GEN	00°19.10'N, 89°56.94'W	Sr/Ca	UM	1332-1359	This paper
SCL1629	SCL	0°41.81'S, 89°15.28'W	$\delta^{18}O$	UM	1420-1447	This paper
SCL1629	SCL	0°41.81'S, 89°15.28'W	Sr/Ca	UM	1420-1447	This paper
SCL1602	SCL	0°50.9'S, 89°33.0'W	$\delta^{18}O$	UM	1129-1167	This paper
SCL1602	SCL	0°50.9'S, 89°33.0'W	Sr/Ca	UM	1129-1167	This paper

*Islands: DAR = Darwin, WLF = Wolf, GEN = Genovesa, URB = Urvina Bay (Isabela), SCL = San Cristobal

[$]Years listed if any portion of the year is included

[@]Labs: UM = University of Michigan, UA = University of Arizona, blank = as described in original reference.

[#]Data have been updated from the original reference as described in supplemental text.

Table S2: U/Th data, Galápagos fossil cores

Sample	^{238}U (ppb)		^{232}Th (ppt)		^{230}Th / ^{232}Th (atomic · 10^{-6})		$\delta^{234}U$ ** (δ-units)		^{230}Th / ^{238}U (activity)		^{230}Th Age (yr) (uncorr.)	^{230}Th Age (yr) (corr.)		$\delta^{234}U_{Initial}$ (δ-units)		^{230}Th Age (yr BP)*** (corr.)
SC1602	3245.2	± 71	302	± 1.0	1586.39	± 5.7	145.06	± 0.36	0.0090	± 0.0000	856 ± 2	854	± 3	145.41	± 0.36	786 ±3
SC1629	2789.1	± 1402,198		± 12	131.93	± 0.6	138.20	± 0.74	0.0063	± 0.0000	606 ± 2	586	± 14	138.43	± 0.74	518 ±14
GEN1601	2484.1	±0.5	209	±0	668.01	±4	142.94	±0.4	0.0034	±0.0000	326 ±2	323	±2	143.07	±0.4	255 ±2
GEN1602	2847.6	±0.4	47	±0	6985.95	±27	143.76	±0.3	0.0070	±0.0000	671 ±2	671	±2	144.03	±0.3	603 ±2
GEN1603	2901.0	±0.7	34	±0	3725.97	±24	144.23	±0.4	0.0026	±0.0000	252 ±1	251	±1	144.33	±0.4	183 ±1
WLF1004	2566.8	±6	36	±3	3478.64	±298	144.58	±3	0.0029	±0.0001	281 ±7	280	±7	144.69	±3	218 ±7
UB0602	2923.5	±2.8	156	±4	1458.37	±46	141.82	±1.5	0.0047	±0.0001	451 ±7	446	±9	142.00	±2	379 ±9

U decay constants: $\lambda_{238} = 1.55125 \times 10^{-10}$ (*73*) and $\lambda_{234} = 2.82206 \times 10^{-6}$ (*66*). Th decay constant: $\lambda_{230} = 9.1705 \times 10^{-6}$ (*66*).

*$\delta^{234}U = ([^{234}U/^{238}U]_{activity} - 1) \times 1000$.

** $\delta^{234}U_{initial}$ was calculated based on ^{230}Th age (T), i.e., $\delta^{234}U_{initial} = \delta^{234}U_{measured} \times e^{\lambda_{234} \times T}$. Corrected ^{230}Th ages assume the initial $^{230}Th/^{232}Th$ atomic ratio of 4.4 ±2.2 $\times 10^{-6}$. Those are the values for a material at secular equilibrium, with the bulk earth $^{232}Th/^{238}U$ value of 3.8. The errors are arbitrarily assumed to be 50%.

***B.P. stands for "Before Present" where the "Present" is defined as the year 1950 A.D.

Table S3: SST characteristics of Galápagos coral sites (OISSTv2, ref. *60)*.

	Urvina Bay	**San Cristobal (NE)**	**San Cristobal (SW)**	**Genovesa**	**Wolf**	**Darwin**
OISST Latitude	0.375°S	0.625°S	0.875°S	0.375°N	1.375°N	1.625°N
OISST Longitude	91.125°W	89.125°W	89.625°W	90.125°W	91.875°W	91.875°W
Mean SST (°C)	23.68	24.10	23.92	24.72	25.53	25.80
Warm month (Mar) SST (°C)	26.63	26.54	26.61	26.86	27.27	27.44
Cool month (Aug*) SST (°C)	21.69	22.37	22.02*	23.38	24.24	24.61
Seasonal SST range (°C)	4.94	4.17	4.59	3.48	3.03	2.84
Std. deviation of SSTA (°C)	1.34	1.30	1.31	1.25	1.11	1.05
Correction factor	1.03	1.00	1.00	0.96	0.85	0.80

*At the San Cristobal-SW site, September is the coolest month by 0.02°C.

Table S4. Calibration slopes and uncertainties

	Monthly resolution		**Annual resolution**	
	Mean slope (per 1°C)	slope error	Mean slope (per 1°C)	slope error
Sr/Ca (mmol/mol)	-0.0597	0.0011	-0.073	0.007
$\delta^{18}O$ (‰)	-0.165	0.004	-0.219	0.025

Table S5. Modern benchmark intervals

Site and core	Start year	End year	Length
Galápagos:			
WLF10-10	1989.75	2009.75	20 yrs
WLF10-06	1989.75	2009.75	20 yrs
WLF10-03	1989.75	2009.75	20 yrs
DAR15-3-2	1991.08	2011.08	20 yrs
N. Line Islands			
Palmyra PRT-10	1995.25	2015.25	20 yrs
Kiritimati 12-6	1990.25	2010.25	20 yrs
Fanning F2	1985.25	2005.25	20 yrs

Table S6. Line Islands core details

Core	Island	Location	Proxy	Years	Reference
FanF5	FAN	3.9°N, 159.2°W	$\delta^{18}O$	1863.46-1887.58	(*74*)
FanF4 Scaled	FAN	3.9°N, 159.2°W	$\delta^{18}O$	1907.46-1943.92	(*74*)
FanA104	FAN	3.9°N, 159.2°W	$\delta^{18}O$	1949.59-1978.75	(*75*)
FanNurhatiF1	FAN	3.9°N, 159.2°W	$\delta^{18}O$	1972.13-1997.71	(*76*)
FanNurhatiF2	FAN	3.9°N, 159.2°W	$\delta^{18}O$	1974.09-2005.54	(*76*)
PalmNB12	PALM	5.87°N, 162.13°W	$\delta^{18}O$	928.25-960.92	(*75*)
PalmL17	PALM	5.87°N, 162.13°W	$\delta^{18}O$	1146.42-1216.92	(*77*)
PalmSB17	PALM	5.87°N, 162.13°W	$\delta^{18}O$	1149.25-1220.09	(*75*)
PalmW23	PALM	5.87°N, 162.13°W	$\delta^{18}O$	1198.58-1249.04	(*77*)
PalmA27	PALM	5.87°N, 162.13°W	$\delta^{18}O$	1242-1330.33	(*77*)
PalmCH9	PALM	5.87°N, 162.13°W	$\delta^{18}O$	1317.25-1406.42	(*75*)
PalmSB7	PALM	5.87°N, 162.13°W	$\delta^{18}O$	1326.67-1357.33	(*75*)
PalmSB5	PALM	5.87°N, 162.13°W	$\delta^{18}O$	1405.25-1448.09	(*75*)
PalmSB6	PALM	5.87°N, 162.13°W	$\delta^{18}O$	1412.09-1443.21	(*75*)
PalmCH5	PALM	5.87°N, 162.13°W	$\delta^{18}O$	1398.75-1463.59	(*75*)
PalmSB3	PALM	5.87°N, 162.13°W	$\delta^{18}O$	1635.09-1666.42	(*75*)
PalmSB13	PALM	5.87°N, 162.13°W	$\delta^{18}O$	1653.75-1695.59	(*75*)
PalmSB8	PALM	5.87°N, 162.13°W	$\delta^{18}O$	1665.09-1703.38	(*75*)
PalmNB9	PALM	5.87°N, 162.13°W	$\delta^{18}O$	1915.25-1937.25	(*75*)
PalmNurhati11	PALM	5.87°N, 162.13°W	$\delta^{18}O$	1886.13-1998.25	(*78*)
PalmPRT10	PALM	5.87°N, 162.13°W	$\delta^{18}O$	1995.08-2016.54	(*74*)
XmasM2	KIRT	2.0°N, 157.3°W	$\delta^{18}O$	1515.75-1561.38	(*79*)
XmasEvans	KIRT	2.0°N, 157.3°W	$\delta^{18}O$	1938.29-1993.58	(*80*)
XmasNurhati09	KIRT	2.0°N, 157.3°W	$\delta^{18}O$	1972.08-1998.38	(*76*)
Xmas12-6	KIRT	2.0°N, 157.3°W	$\delta^{18}O$	1986.42-2011.92	(*29*)

*Islands: PALM = Palmyra, KIRT = Kiritimati (Christmas); FAN = Fanning

Table S7. Model ensembles and confidence limits (NCAR CESM1.2)

	Comparison	Forcing	Span	Ensemble	Years	90% CI	95% CI
1	Change relative to PI (forced; fig. 4)	All natural	850-1850 CE (1000 yrs)	11	Coral years only	28%	36%
2	Change relative to PI (control; fig. S13)	None (control)	1155 yrs	1	Coral years only	21%	30%
3	Change relative to PI (forced)	All natural	850-1850 CE (1000 yrs)	11	All years	34%	42%
4	Change relative to PI (control)	None (control)	1155 yrs	1	All years	34%	42%
5	Change relative to PI control (all ensemble members together, fig. S13)	All natural + anthro-pogenic (RCP8.5)	850-2100 CE (1250 yrs)	4	All years	26%	33%